



Article

Global Dynamic Landslide Susceptibility Modeling Based on ResNet18: Revealing Large-Scale Landslide Hazard Evolution Trends in China

Hui Jiang ^{1,2} , Mingtao Ding ^{1,3,4,5,*} , Liangzhi Li ⁶ and Wubiao Huang ⁷

¹ College of Geological Engineering and Geomatics, Chang'an University, Xi'an 710054, China; 2022126019@chd.edu.cn

² Big Data Center for Geosciences and Satellites, Chang'an University, Xi'an 710054, China

³ Key Laboratory of Loess, Xi'an 710054, China

⁴ Key Laboratory of Western China's Mineral Resource and Geological Engineering, Ministry of Education, Xi'an 710054, China

⁵ Generic Technical Development Platform of Shaanxi Province for Imaging Geodesy, Xi'an 710021, China

⁶ School of Land Engineering, Chang'an University, Xi'an 710064, China; liliangzhi@chd.edu.cn

⁷ School of Geodesy and Geomatics, Wuhan University, Wuhan 430079, China; huangwubiao@whu.edu.cn

* Correspondence: mingtaoding@chd.edu.cn

Abstract: Large-scale and long-term landslide susceptibility assessments are crucial for revealing the patterns of landslide risk variation and for guiding the formulation of disaster prevention and mitigation policies at the national level. This study, through the establishment of a global dynamic landslide susceptibility model, uses the multi-dimensional analysis strategy and studies the development trend of China's large-scale landslide susceptibility. First, a global landslide dataset consisting of 8023 large-scale landslide events triggered by rainfall and earthquakes between 2001 and 2020 was constructed based on the GEE (Google Earth Engine) platform. Secondly, a global dynamic landslide susceptibility model was developed using the ResNet18 (18-layer residual neural network) DL (deep learning) framework, incorporating both dynamic and static LCFs (landslide conditioning factors). The model was utilized to generate sequential large-scale landslide susceptibility maps for China from 2001 to 2022. Finally, the MK (Mann–Kendall) test was used to investigate the change trends in the large-scale landslide susceptibility of China. The results of the study are as follows. (1) The ResNet18 model outperformed SVMs (support vector machines) and CNNs (convolutional neural networks), with an AUC value of 0.9362. (2) SHAP (Shapley Additive Explanations) analyses revealed that precipitation played an important factor in the occurrence of landslides in China. In addition, profile curvature, NDVI, and distance to faults are thought to have a significant impact on landslide susceptibility. (3) The large-scale landslide susceptibility trends in China are complex and varied. Particular emphasis should be placed on Southwest China, including Chongqing, Guizhou, and Sichuan, which exhibit high landslide susceptibility and notable upward trends, and also consider Northwest China, including Shaanxi and Shanxi, which have high susceptibility but decreasing trends. These results provide valuable insights for disaster prevention and mitigation in China.



Academic Editor: Tiago Filipe da Silva Miranda

Received: 12 January 2025

Revised: 8 February 2025

Accepted: 12 February 2025

Published: 15 February 2025

Citation: Jiang, H.; Ding, M.; Li, L.; Huang, W. Global Dynamic Landslide Susceptibility Modeling Based on ResNet18: Revealing Large-Scale Landslide Hazard Evolution Trends in China. *Appl. Sci.* **2025**, *15*, 2038.

<https://doi.org/10.3390/app15042038>

Copyright: © 2025 by the authors. Licensee MDPI, Basel, Switzerland. This article is an open access article distributed under the terms and conditions of the Creative Commons Attribution (CC BY) license (<https://creativecommons.org/licenses/by/4.0/>).

Keywords: dynamic landslide susceptibility; ResNet18; Mann–Kendall test; landslide conditioning factors

1. Introduction

Catastrophic landslides, as profound natural calamities, exert ruinous impacts on property and claim lives across the world [1,2]. They result from various natural and human-induced factors, including heavy rainfall, snowmelt, earthquakes, fluctuating water levels, natural erosion, weathering processes, and human activities such as improper land use and engineering projects [3–5]. Landslides can severely impact infrastructure while also directly endangering human lives. Froude and Petley report that between 2004 and 2016, 4862 fatal landslides claimed up to 55,997 lives globally [6]. This alarming figure underscores the enormous threat that landslides pose to society. Furthermore, landslides exhibit remarkable spatial heterogeneity. The risk and frequency of landslides vary differently across regions. This geographical specificity makes the impact of landslide hazards on specific areas particularly significant. Therefore, it is imperative to engage in comprehensive research and to apply effective risk management strategies in areas characterized by high levels of risk. LSM (landslide susceptibility mapping) serves as a vital tool for disaster risk assessment, helping to identify vulnerable areas through detailed analysis and mapping, offering a strong scientific basis for informed decisions on disaster prevention and mitigation [7,8].

Recent advances in DL (deep learning) have demonstrated substantial potential for LSM, with CNNs (convolutional neural networks) emerging as particularly effective tools for capturing spatial patterns and complex correlations inherent in geospatial data [9,10]. Ge [11] conducted a comprehensive evaluation of various CNN architectures for landslide susceptibility assessment, comparing their performance with traditional ML (machine learning) and DL techniques, and affirmed the reliability of CNN-based approaches in LSM. Despite their success, these models often encounter significant challenges, including overfitting, computational inefficiency, and limited generalization across diverse geographic regions. Although traditional CNN architectures are highly effective, they face difficulties in learning complex, hierarchical features, especially in the presence of limited labeled data or suboptimal data quality. To mitigate these issues, the present study utilizes ResNet18, a variant of the ResNet (residual network) architecture, which incorporates residual learning to facilitate the training of deeper networks while addressing the vanishing gradient problem. This distinctive feature of ResNet18 enables it to efficiently model intricate spatial dependencies in LSM tasks, even when faced with data sparsity or noisy inputs [12]. Furthermore, ResNet18's computational efficiency and its established success in a wide range of image-based tasks make it a highly suitable choice for LSM. In LSM, both predictive accuracy and the optimization of computational resources are paramount, and ResNet18 excels in addressing these requirements [13].

LSM has been a subject of significant interest in the academic community, evolving from early theoretical debates to its latest practical applications. It has evolved from a single analysis of natural factors to a comprehensive analysis of multiple factors, and its research methodology and technical methods have been constantly refined and developed. The data presented in Table 1 indicate that the field of landslide susceptibility research has expanded to the national and global scales. According to the analyses by Emberson [14] and Lin [15] of large-scale and long-term landslide risk, the importance of conducting landslide studies at large spatial and temporal scales is evident. Lan's [16] research emphasizes that geological, geomorphological, and climatic processes (including disaster processes) are interrelated across regional and multi-temporal scales. Therefore, conducting systematic assessments of major disaster risks, such as catastrophic landslides, over large regions and extended time periods is of paramount importance.

Furthermore, investigating landslide susceptibility by analyzing factor-induced landslides and integrating dynamic factors is an important area of current disaster early warning,

prevention, and mitigation research [17]. Kirschbaum [18] developed a web-based platform for assisting decision making to assess the potential landslide activity in real-time. Lee [19] created a system dynamics model to examine the complex relationship between rainfall patterns and spatial vulnerability. By incorporating real-time rainfall data and adjusting previous rainfall periods, it enhances the accuracy of predicting landslide warning times and potential locations. Liu [20] unveiled a fresh approach for the early detection of landslides in dynamic susceptibility analysis. The approach utilizes a blend of SBAS-InSAR data based on time series along with static conditional variables to establish an LSM model. This produced various LSM tools over time, enabling the spatiotemporal assessment of landslide susceptibility within the research area. Lin [21] introduced a strategy for conducting a dynamic analysis of landslide susceptibility within a research region by focusing on the dynamic influence of land use. Meanwhile, neural networks have been widely applied in temporal landslide prediction. For example, Mondini [22] used DL for predicting shallow landslides triggered by rainfall. Distefano [23] employed artificial neural networks to study the impact of rainfall and soil moisture on the landslide trigger threshold. Additionally, Nocentini [24] used ML for spatiotemporal landslide probability assessment in the Kvam (Norway). Therefore, it is important to use neural networks for landslide temporal prediction and evaluation.

In conclusion, these studies provide valuable insights into both large-scale and dynamic LSM. However, most current studies on large-scale dynamic landslide susceptibility focus on a single dynamic factor and employ a simple ML method [21,25,26]. Therefore, the study uses the ResNet18 to develop a global dynamic landslide susceptibility model that includes precipitation, land cover type, and the NDVI (Normalized Differential Vegetation Index) as dynamic condition factors, combined with elevation, aspect, slope, profile curvature, the TRI (Terrain Roughness Index), plane curvature, distance to faults, lithology, and surface soil taxonomy. China, recognized as one of the nations with the highest incidence of landslides globally, was selected as the focus of the study. The contributions of the study are organized into three components. Firstly, a dynamic landslide susceptibility model was employed to assess large-scale landslide susceptibility across China over a period of 22 years, from 2001 to 2022. Secondly, the landslide susceptibility trends in China during this timeframe were tested using the MK (Mann–Kendall) test method. A time series analysis of representative regional points was conducted to clarify the evolving trends of landslide hazards that have occurred in the country over the past 22 years. Thirdly, this study explained the model through SHAP (Shapley Additive Explanations) and revealed the effect of conditional factors on dynamic landslide susceptibility. This research provides a scientific basis for decision makers to create effective adaptation strategies and serves as a valuable reference for landslide hazard warning, prevention, and mitigation.

Table 1. Statistical overview of landslide susceptibility studies conducted nationally and globally.

Year of Research	Main Researchers	Space Scale	Space Resolution	Methodology	Evaluation Type	Main Findings
2013	Liu [27]	National (China)	1 km × 1 km	Artificial neural network model	Static	Identified high-risk areas across China
2017	Stanley [28]	Global	1 km × 1 km	A heuristic fuzzy approach	Static	Developed a global landslide susceptibility map
2018	Liu [29]	National (China)	1 km × 1 km	Logistic regression model	Static	Evaluation of landslide hazards, vulnerabilities, and risks in China
2021	Lin [30]	National (China)	1 km × 1 km	GAM (generalized additive model) and GAMM (generalized additive mixed model)	Static	Assessing the vulnerability to landslides triggered by rainfall in China

Table 1. *Cont.*

Year of Research	Main Researchers	Space Scale	Space Resolution	Methodology	Evaluation Type	Main Findings
2021	Wang [31]	National (China)	1 km × 1 km	The maximum entropy model	Static	Evaluated susceptibility and risk factors of landslides in China
2022	Lin [15]	National (China)	1 km × 1 km	GAMM	Static	Evaluation of landslide susceptibility in China in relation to climate change is proposed
2022	Li [25]	Global	1 km × 1 km	Random forest and LightGBM model	Dynamic (2020–2021)	Created a global dynamic landslide susceptibility model
2024	(This text)	National (China)	1 km × 1 km	ResNet18 model	Dynamic (2001–2022)	Revealed dynamic changes in landslide susceptibility in China from 2001–2022

2. Study Area and Resources

2.1. Study Area

Landslides are common natural disasters caused by various factors, including topography, geomorphology, geological structure, hydrometeorological, and human activities. In recent years, landslides have increased in frequency with global climate change, rising global temperatures, and heightened precipitation levels. China, acknowledged as one of the countries most prone to landslide disasters worldwide, has been chosen as the focal point of this study.

China is located in eastern Asia with the Pacific Ocean to its east. It encompasses a vast area with diverse natural environments. China covers an extensive land area of around 9.6 million square kilometers, along with a maritime zone measuring 4.73 million square kilometers. The geographical coordinates of China range from 73°33' E to 135°05' E and 3°51' N to 53°33' N (Figure 1). The geographical features of China are characterized by significant elevation variations, with the western regions exhibiting high altitudes and the eastern regions presenting lower elevations. Plateaus, hills, and mountains dominate the landscape, covering approximately 67% of the country, while the remaining 33% consists of plains and basins. The geological structure is characterized by multiple plates, fracture zones, and folded zones. The climate is diverse, ranging from cold temperate to temperate, subtropical, and tropical. Its complex topography, diverse geological structures, variable climate, and human activity have led to frequent landslide disasters in China.

2.2. Resources

2.2.1. Landslide Inventory

Landslide inventories represent a fundamental dataset for LSM studies and contain temporal and spatial information on landslides. The primary data source for global landslide susceptibility research is the COOLR (Cooperative Open Online Landslide Repository), which includes datasets such as the Landslide Report Catalogue [32] and GLC (Global Landslide Catalogue) [33,34] and a subset of locally reported landslide data (<https://landslides.nasa.gov>, accessed on 1 April 2024) (Figure 2). The website contains data on landslide sites from 1915 to 2021 sourced from various sources, including satellite remote sensing, ground surveys, and disaster reports. The integration of these datasets enabled the exclusion of small landslides, landslides with ambiguous temporal information, and landslides with incomplete data. A total of 8023 large-scale landslide events triggered by rainfall and earthquakes between 2001 and 2020 were extracted. This was performed because rain and earthquakes are the most common high-impact landslide triggers globally, and high-quality data on rain and earthquakes are relatively abundant and readily available. These data serve as a solid foundation for investigating landslide susceptibility, thereby

improving the comprehension of both the spatiotemporal patterns of landslide events and their associated triggers.

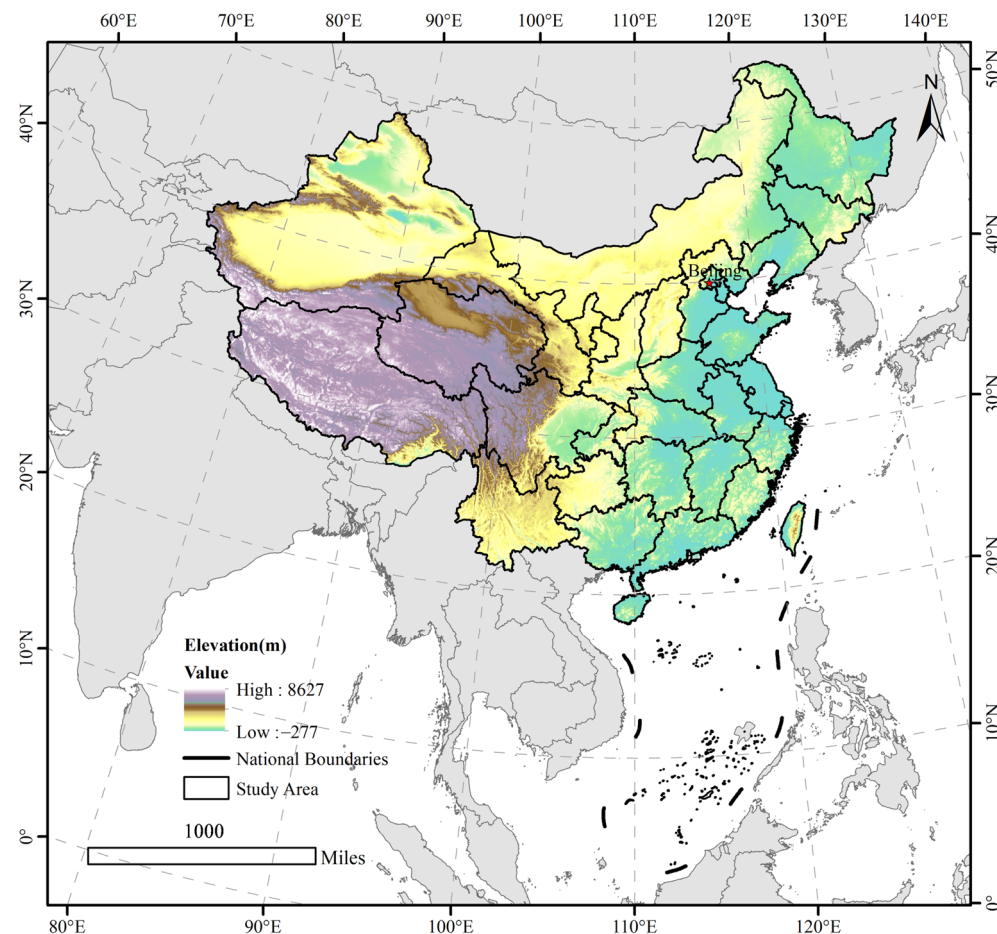


Figure 1. Geomorphological zoning in China.

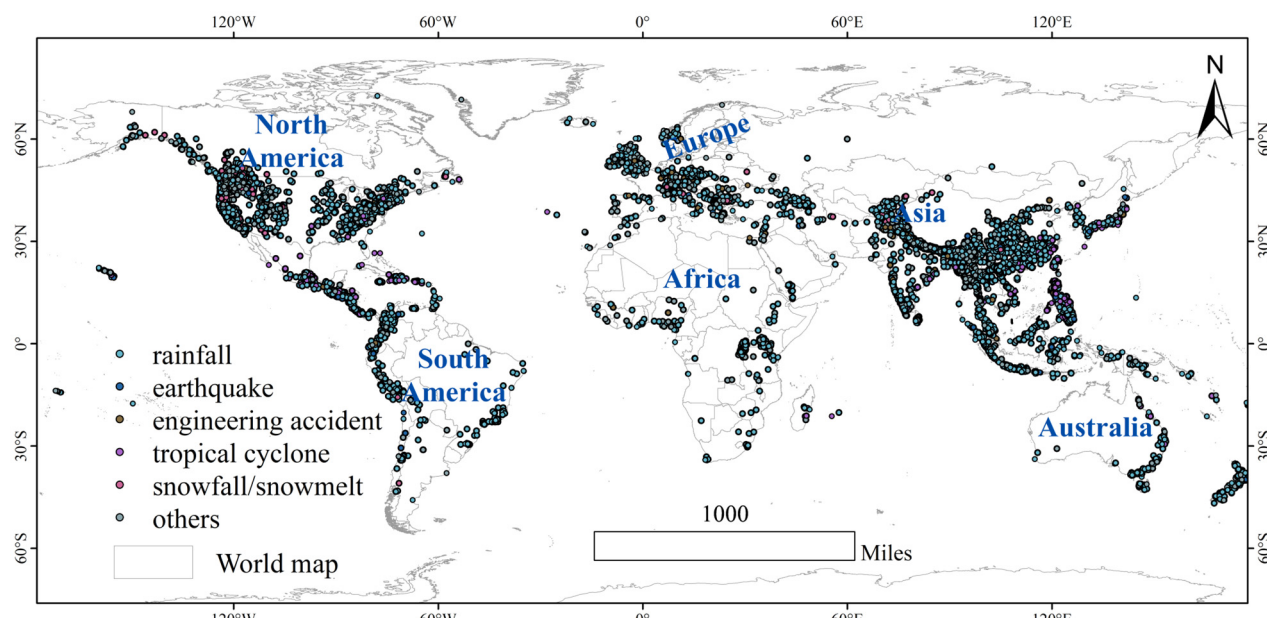


Figure 2. Global landslide distribution.

2.2.2. Landslide Conditioning Factors

LCFs (Landslide conditioning factors) encompass both natural and anthropogenic elements that affect the possibility of landslide events, which is critical for the precise assessment of landslide susceptibility [30,35–37]. However, there are no unified standards for the selection and application of LCFs. By summarizing a massive body of literature [25,27,28,38], it was found that topography, geological, soil, and environmental factors are the most commonly used LCFs in global studies. From the studies, we selected for 12 LCFs. The dynamic condition factors were derived from time-based data encompassing NDVI, land cover type, and precipitation. Static condition factors were extracted from a range of data sources including aspect, elevation, slope, profile curvature, TRI, lithology, plane curvature, distance to faults, and surface soil taxonomy data. Table 2 presents a detailed enumeration of all data sources utilized.

Table 2. Statistics on data sources.

Data Type	Conditioning Factor	Dataset	The State of the Condition Factor
Topographic	Elevation (ELE)	GMTED2010 (Global Multi-resolution Topographic Elevation Data 2010) model is characterized by a spatial resolution of 7.5 arcseconds	Static
	Slope (SL)		
	Aspect (AS)		
	Plane curvature (PLC)		
	Profile curvature (PRC)		
Geological	Terrain Roughness Index (TRI)	GLIM (Global Lithology Map), Resolution 1:3750,000	Static
	Lithology (LITHO)		
	Distance to faults (FTD)		
Soil	Surface soil taxonomy (SST)	OpenLandMap USDA soil classification, Resolution 250 m	Static
Environmental	Normalized Difference Vegetation Index (NDVI)	Global MOD13Q1 V6 Vegetation Index, Resolution 250 m	Dynamic
	Land cover type (LC)	Global MCD12Q1 V6 land cover type, resolution 500 m	
	Annual cumulative precipitation (PRE)	ERA5-Land Monthly Aggregated-ECMWF climate analysis dataset, resolution 0.1°	

Topographic factors are essential components in the analysis of LSM and play a substantial role in influencing the formation and spatial distribution of landslides. These factors, which encompass slope, aspect, and elevation, represent the variations in the terrain's surface characteristics. They function as direct indicators of the essential conditions related to slope instability and have a substantial effect on the frequency and distribution of landslides. Therefore, this study examines aspect, slope, elevation, TRI, profile curvature, and plane curvature. Elevation data were sourced from the GMTED2010 [39], and other terrain factors were calculated from the elevation data.

Among the geological factors, lithology is intrinsically linked to slope stability, with variations in lithological composition influencing the magnitude of landslides. The lithological information utilized in this research is sourced from the GLIM [40]. The susceptibility to landslides is significantly influenced by geological formations, with faults playing a crucial role. Joint fractures formed by faults often determine the potential sliding surfaces and boundary conditions of landslides, which are particularly susceptible to destabilization in areas with complex geological formations. This study further obtained distance data from the landslide point to the fault from the fault dataset of the GEM Global Active Faults Project [41]. (<https://github.com/GEMScienceTools/gem-global-active-faults>, accessed on 1 April 2024).

Among the soil factors, surface soil taxonomy has a significant influence on landslides through its effects on water retention and permeability, the stability of the soil cover, and its interaction with lithology. Consequently, it is considered one of the primary contributors to landslide occurrences [42]. In this study, the OpenLandMap USDA Soil Taxonomy Great Groups were selected and visualized using [OpenLandMap.org](#).

Among the environmental factors, the NDVI serves as an indicator of vegetation cover, illustrating the extent of vegetative presence within a specified area. Vegetation mainly reduces the damage of water flow to the slope through the root stabilization of its rhizomes, thereby helping to prevent landslides [43]. NDVI data were sourced from the MOD13Q1 Version 6 dataset with a time resolution of 16 days. Various land cover types exhibit distinct soil mechanical and hydrological characteristics, which influence slope stability and, thus, landslide development. As a result, land cover types were frequently chosen as a focus for investigating landslide susceptibility [44]. Land cover type data were sourced from the MCD12Q1 Version 6 dataset with a time resolution of 1 year. Landslides are primarily triggered by precipitation, which facilitates the infiltration of rainwater into soil and rock formations. This infiltration alters the physical properties of these materials, thereby diminishing their resistance to sliding. When the shear strength of the soil is insufficient to resist gravitational forces or other external stresses, the stability of the slope is compromised, leading to landslides [38]. Precipitation data were analyzed using the ERA5-Land Monthly Aggregated-ECMWF climate reanalysis dataset with a temporal resolution of monthly average data [45].

3. Methodology

Figure 3 depicts the fundamental steps involved in developing and assessing a dynamic landslide susceptibility model. This includes the following steps. (1) Data preprocessing was performed, which included a review of the relevant literature, the collection of landslide inventory data, and the preliminary selection of static and dynamic conditioning factor data, followed by data preprocessing. (2) Conditioning factor selection was conducted utilizing the *PCC* (Pearson correlation coefficient) and *MI* (mutual information). This was followed by selecting the factors that triggered the landslides and constructing a model training dataset. (3) Model construction and evaluation was performed using three methods—SVM (support vector machines), CNN, and ResNet18—for model construction. The model's performances were assessed utilizing various model evaluation metrics. (4) Dynamic factor change analysis was conducted by using the MK test to test the spatial distribution and analyze the spatial trend change of dynamic factors in China. A model interpretability analysis was performed utilizing the SHAP method. The results and analysis of dynamic landslide susceptibility were conducted. The most performant model was employed to evaluate dynamic landslide susceptibility for the chosen study area, and the susceptibility probability map was partitioned using the equal-interval method. The dynamic landslide susceptibility prediction probability results were subjected to the MK test, and typical areas (significantly increasing, decreasing, high, and extremely high landslide susceptibility zoning) were analyzed in a time series using the one-dimensional linear regression method.

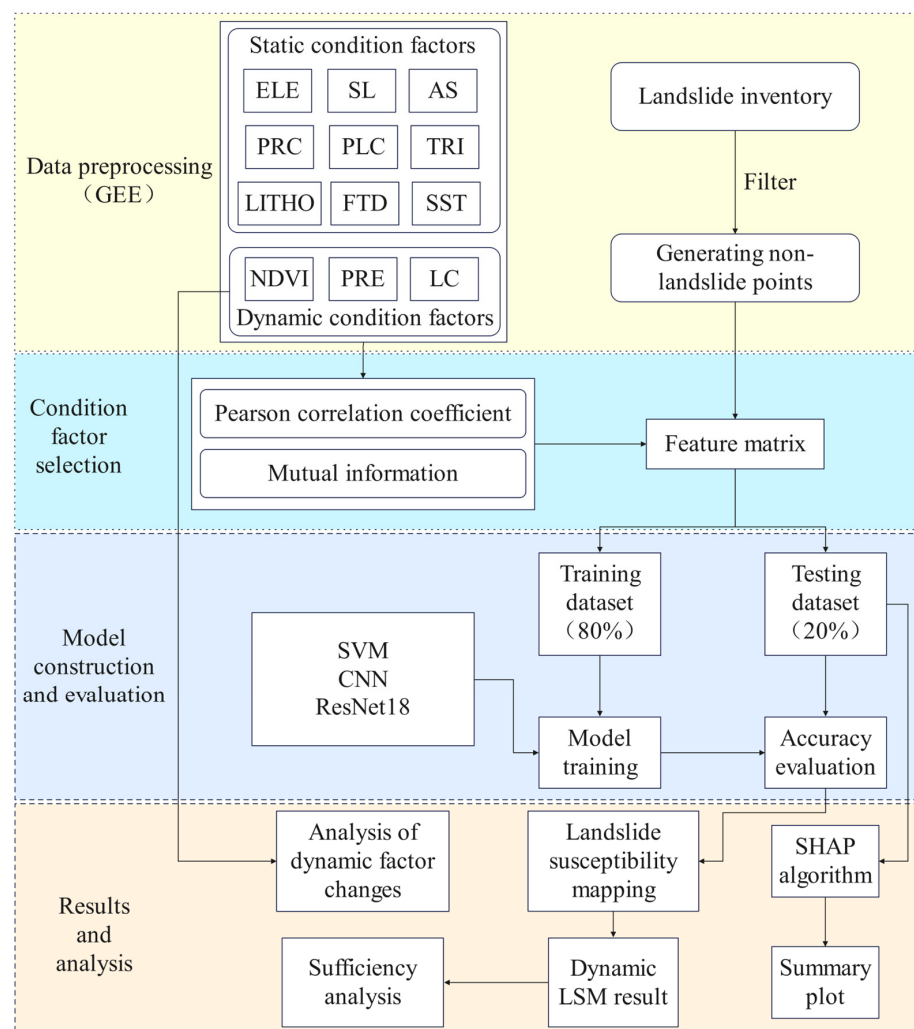


Figure 3. Dynamic landslide susceptibility evaluation process.

3.1. Data Preprocessing

GEE (Google Earth Engine) serves as an online platform for geographic information processing that integrates a large amount of remotely sensed and geospatial data to provide users with high performance data processing and analysis capabilities [46,47]. The GEE platform was utilized to handle various conditional factors such as standardizing spatial resolution, identifying dynamic factors, and overlaying factor data. A feature matrix was generated using the landslide inventory data. According to Huang [48] and Pourghasemi [49], the data imbalance issue suggests that employing a one-to-one ratio of landslide-to-non-landslide samples is not entirely justifiable, given that the actual landslide area represents only a minor fraction of the total regional area. Recognizing this problem, the feature matrix of this study was constructed employing a 1:2 ratio containing 8023 landslide and 16,046 non-landslide samples. To process the impact factors, the vector data were rasterized into $1 \text{ km} \times 1 \text{ km}$ resolution cells. To ensure consistent spatial resolution throughout the dataset, the raster data were all sampled as $1 \text{ km} \times 1 \text{ km}$ resolution cells. In addition, to ensure consistency and comparability in the temporal analysis, it is important to consider that precipitation data are typically available at monthly scales. NDVI data, derived from satellite imagery, are processed at a seasonal scale. Land cover data is updated annually, thus necessitating the use of a consistent annual temporal resolution across all factors. While finer temporal resolutions could offer better insights into short-term landslide triggers, using an annual resolution allows for the analysis of broader, long-term

trends in landslide susceptibility and land system dynamics. Studies by Lin [30] and Ngo [50] have used similar temporal resolutions to effectively model large-scale landslide susceptibility, emphasizing that annual data are generally sufficient for understanding long-term susceptibility patterns.

Subsequently, landslide and non-landslide data are integrated with the impact factors to create a dataset. To ensure the scientific rigor and reliability of the model, the dataset is randomly partitioned into a training set and testing set, with a 4:1 ratio. This approach helps maintain the representativeness and independence of the data for model validation.

3.2. Condition Factor Selection

In landslide susceptibility evaluations, the *PCC* serves as a significant metric for analyzing the relationship among conditional factors. A *PCC* value nearing an absolute value of 1 signifies a more robust correlation between the two variables being analyzed [9,51]. In the DL training, high-correlation data not only causes data redundancy and reduces model execution efficiency, but it also has an impact on prediction accuracy. However, correlation analysis does not analyze the dependency between the character variable (LCFs) and the dependent variable (landslide class label) to select the appropriate condition factor that triggers landslides. Given this issue, the study employed the *MI* to evaluate the association between the predictors and the outcome variables. Finally, the *PCC* and *MI* were combined to choose the LCFs.

PCC includes the conditional factors *E* and *F*, and the *PCC(E, F)* of *E* and *F* is defined as follows:

$$PCC(E, F) = \frac{\sum_{i=1}^n (E_i - \bar{E})(F_i - \bar{F})}{\sqrt{\sum_{i=1}^n (E_i - \bar{E})^2} \sqrt{\sum_{i=1}^n (F_i - \bar{F})^2}}, \quad (1)$$

where E_i and F_i denote the i th conditional factor layer of *E* and *F*, respectively, while \bar{E} and \bar{F} denote the sample averages of *E* and *F*. According to *PCC* [52], if $PCC > 0.7$, the variables are strongly correlated, warranting consideration for exclusion from further analysis.

MI includes the condition factor *E* and landslide type variable *G*, and the *MI(E, G)* of *E* and *G* is defined as follows:

$$MI(E, G) = \sum_{g \in G} \sum_{e \in E} p(e, g) \log \left(\frac{p(e, g)}{p(e)p(g)} \right), \quad (2)$$

where $p(e, g)$ denotes the joint probability density function of the stochastic variables *E* and *G*, $p(e)$ and $p(g)$ denotes the edge probability density functions of *E* and *G*, respectively. According to the properties of *MI* [53], the properties of *MI* indicate that an increase in the mutual information value signifies a stronger dependence between the features and the label classes.

3.3. Model Construction and Evaluation

3.3.1. Construction of the Dynamic Landslide Susceptibility Evaluation Model

The SVM constitutes a significant supervised learning approach for evaluating hazard susceptibility. It aims to identify the optimal decision boundary to distinguish positive and negative samples within a training dataset [54,55]. SVMs are frequently employed in LSM owing to their accuracy, robustness, and generalization ability [56], making them the comparison model for this study.

CNNs are among the most popular DL algorithms and have attracted attention for their superior performance in image vision [50,57]. Th CNN is mainly composed of convolution, pooling, activation, and a fully connected layer (Figure 4a). The convolutional layer plays a crucial role in capturing spatial hierarchies and identifying complex relationships

between different features within the input data, thereby enhancing the network's ability to extract meaningful representations. The output of the convolutional layer is subsequently processed by the activation layer, where the ReLU (rectified linear unit) activation function is commonly employed. The ReLU effectively introduces nonlinearity into the model, significantly improving its capacity for complex pattern recognition. The pooling layer follows, performing downsampling to reduce the dimensionality of the feature maps, thereby mitigating the risk of overfitting and improving model generalization. Finally, the fully connected layer integrates the pooled features to produce the final output. CNNs are extensively applied in landslide susceptibility modeling due to their robust feature extraction capabilities, ability to learn spatial patterns, and parameter-sharing mechanism, which significantly reduces the computational complexity of large-scale datasets.

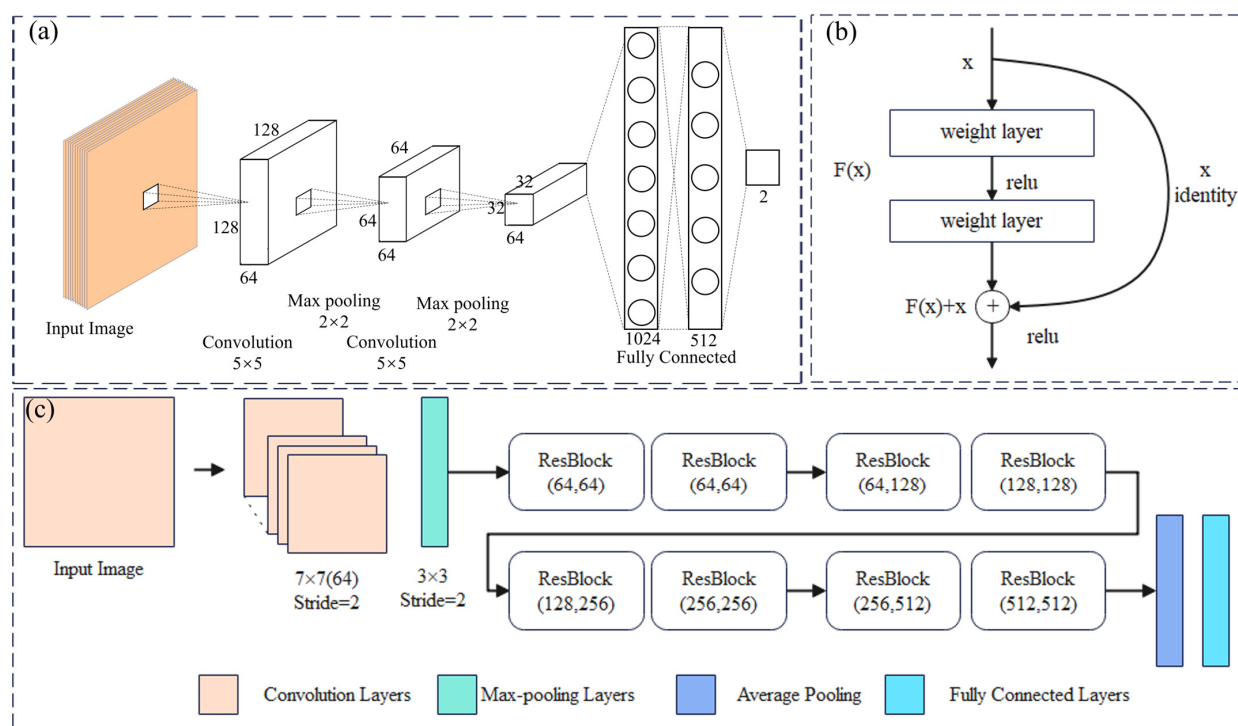


Figure 4. The network architecture. **(a)** The CNN network architecture, **(b)** the residual unit, and **(c)** the ResNet18 network architecture.

ResNet is a sophisticated deep CNN designed to address gradient vanishing and network degradation during training. This was proposed by He [13] at Microsoft Research in 2015; its fundamental unit is the ‘residual block’. Each block includes multiple cascaded convolutional layers, activation functions, and batch normalization. The output encompasses two distinct components: One is an unprocessed direct result derived from input data x , known as shortcut or skip connection, and the other component represents $F(x)$ added together as $x + F(x)$. This process facilitates effective information transfer across various network layers, mitigating vanishing gradients. ResNet involves the repetitive stacking of these residue units, leading to diverse types such as ResNet18, ResNet34, and ResNet50.

This study utilizes landslide susceptibility data that encompass a diverse array of high spatial resolution datasets, including key indicators such as the NDVI, DEMs (digital elevation models), and other geospatial layers. These datasets exhibit complex spatial patterns that are essential for the precise modeling of landslide susceptibility. The architecture of ResNet18, with its residual connections, is particularly well-suited for capturing these complex spatial dependencies, enabling the model to learn hierarchical features effectively.

while mitigating the vanishing gradient problem, even when processing high-resolution spatial data. Furthermore, the global scope of the study necessitated the use of a large, diverse dataset with numerous input features derived from heterogeneous data sources. In comparison to deeper neural network architectures, ResNet18's relatively lightweight design offers advantages. It allows for efficient training on large-scale datasets without imposing excessive computational demands. This ensures that the model can be deployed over extensive geographic areas without compromising processing time or memory capacity. Additionally, the temporal variability of landslide events, such as fluctuations in susceptibility due to dynamic environmental factors like rainfall, requires the model to generalize effectively across different time periods. While ResNet18 is predominantly an image-based architecture, its capacity to handle spatial features with temporal variability—when combined with time-sensitive input layers—makes it a strong candidate for modeling dynamic susceptibility over time. Consequently, ResNet18 offers a compelling combination of spatial efficiency, computational feasibility, and adaptability to temporal changes. This makes it an ideal choice for global landslide susceptibility modeling, where both accuracy and scalability are critical.

To this end, ResNet18 was selected for simulating landslide susceptibility in this study. For comparative analysis, SVM and CNN models were also considered. The residual units and the ResNet18 network architecture are illustrated in Figure 4b,c.

3.3.2. Model Evaluation

The evaluation of model performance is a crucial step in constructing DL models. Various metrics must be employed to obtain an accurate and comprehensive evaluation of the model. In binary classification tasks, the most suitable evaluation metrics are derived from confusion matrices. These include the accuracy, f1-measure, recall, precision, ROC (receiver operating characteristic) curve, and AUC (area under the ROC). A higher proximity of these metric values to 1 indicates a greater efficacy of the model in fulfilling its designated objectives. Among the various evaluation metrics, the AUC is commonly employed to assess the performance of landslide susceptibility models. In the ROC curve, the horizontal axis represents the FPR (false positive rate), while the vertical axis corresponds to the TPR (true positive rate). This curve provides a comprehensive assessment of the model's performance by simultaneously evaluating its sensitivity and specificity. The calculation formulas of various evaluation indicators are shown in Table 3.

Table 3. Performance evaluation indicators for evaluating binary classification DL models.

Metric	Formula	Remark
Accuracy	$\frac{TN+TP}{TP+FP+FN+TN}$	The ratio of accurately predicted landslide sample points to the total number of sample points.
Precision	$\frac{TP}{TP+FP}$	False detection rate, the ratio of accurately predicted landslide positive sample points to the overall number of predicted positive sample points.
Recall	$\frac{TP}{TP+FN}$	Missed detection rate, the ratio of accurately predicted positive sample points for the landslide corresponds to the total number of positive sample points identified.
F1-measure	$\frac{2TP}{2TP+FP+FN}$	The integrated means of precision and recall.
AUC	The integral of the ROC curve	Careful consideration of landslide points with the landslide classification ability can overcome sample imbalance.
TPR	$\frac{TP}{TP+FN}$	The proportion of positive samples classified as positive.
FPR	$\frac{FP}{FP+TN}$	The proportion of negative samples classified as positive.

Notes: TP denotes a sample identified as a landslide that is accurately predicted as such. FP denotes a non-landslide sample that is incorrectly predicted as a landslide. TN denotes a sample classified as a non-landslide that is correctly predicted as a non-landslide. FN denotes a landslide sample that is incorrectly identified as a non-landslide.

3.4. Result Analysis: SHAP Explainable and MK Test Method

3.4.1. SHAP Explainable

The SHAP model interpretation tool was initially proposed by economist Lloyd Shapley and originated from a game theory [58]. With Lundberg [59] introducing this concept into the field of ML, SHAP helps reveal the results of black-box models and improves model transparency and user's trust in ML models. Furthermore, Pradhan's initial use of SHAP in landslide susceptibility modeling has gradually led to an increased focus on model interpretability in LSM [60].

The SHAP value serves to quantify the contribution of each feature to the model, thereby facilitating a deeper understanding of the role that these features play within the model. The SHAP is computed as follows:

$$\phi_i = \sum_{S \subseteq \{x_1, \dots, x_p\} \setminus \{x_i\}} \frac{|S|!(p-|S|-1)!}{p!} [f_x(S \cup \{x_i\}) - f_x(S)], \quad (3)$$

where ϕ_i denotes the contribution of the i th feature, S denotes the collection of all features excluding feature x_i , and p indicates the overall number of features. The $f_x(S \cup \{x_i\})$ indicates the model predicted value when features are added on top of the subset of features S , and $f_x(S)$ represents the model predicted value when only the subset of features S is used.

The interpretation of SHAP includes global and local interpretations, with Shapley values serving as an additive feature attribution method. Each observation model displays a Shapely value, resulting in each characteristic displaying a particular shape. For a specific input feature z , local accuracy requires that the interpreted model's output matches the output of the reduced input z' , as given by the following equation:

$$f(z) = g(z') = \phi_0 + \sum_{i=1}^M \phi_i z'_i, \quad (4)$$

where g denotes the explanatory model, $z' \in \{0, 1\}^M$ denotes the simplified z input features, M signifies the overall number of input features, and ϕ_i is as derived from Equation (3). ϕ_0 denotes the model output in the absence of all features. For a global interpretation, the average impact of each feature was obtained by averaging the SHAP values for all samples.

In this study, we used SHAP to easily estimate the influence of various features on DL models [61,62]. First, we create a DL SHAP "Explainer" object that uses training samples as background data. Then, the characteristics of the test samples are interpreted and analyzed. Finally, we generate a summary plot that shows the importance ranking of each feature. This methodology not only offers a comprehensive analysis of each feature's contribution to the predicted outcomes but also enhances the accuracy and dependability of model interpretations.

3.4.2. MK Test

The MK test is a non-parametric statistical method used to analyze trends in time-series data [63,64]. It employs p -values and Z-values to ascertain the presence of significant trends in the dataset. The research employs the MK test to analyze the trend of landslide susceptibility probability over a span of 22 years in China. Specifically, while $Z < 0$ signifies a downward trend, Z equals zero signifies the absence of a significant trend, and $Z > 0$ signifies an upward trend. The significance level, represented by p , reflects the probability of erroneously rejecting the null hypothesis. For a significance level of $p = 0.01$, the confidence level is 2.58, whereas for $p = 0.05$, the confidence level is 1.96. In the study, when $0.01 < p < 0.05$ and $1.96 < |Z| < 2.58$, a trend is regarded as significant, while a trend is

considered highly significant if $p < 0.01$ and $|Z|$ exceeds 2.58. In all other cases, the trend is viewed as not significant.

4. Results

4.1. LCFs Selection and Dynamic Factor Change Trend Analysis in the Study Area

4.1.1. LCFs Selection and Analysis

In this study, we first chose 12 variables: elevation, aspect, slope, profile curvature, plane curvature, TRI, NDVI, land cover type, surface soil taxonomy, precipitation, lithology, and distance to faults. The *PCC* between the LCFs was calculated, with the results depicted in Figure 5. The correlation coefficient between the slope and profile curvature was determined to be 0.725, suggesting a robust association between these two variables. Furthermore, we calculated the *MI* between the LCFs and landslides, with the results illustrated in Figure 6. The results indicate that the slope has less information and is less dependent on landslide occurrence. The slope factor was eliminated after careful consideration. After factor elimination, eleven factors, including elevation, aspect, profile curvature, plane curvature, TRI, NDVI, distance to faults, land cover type, surface soil taxonomy, precipitation, and lithology, were retained for the final model.

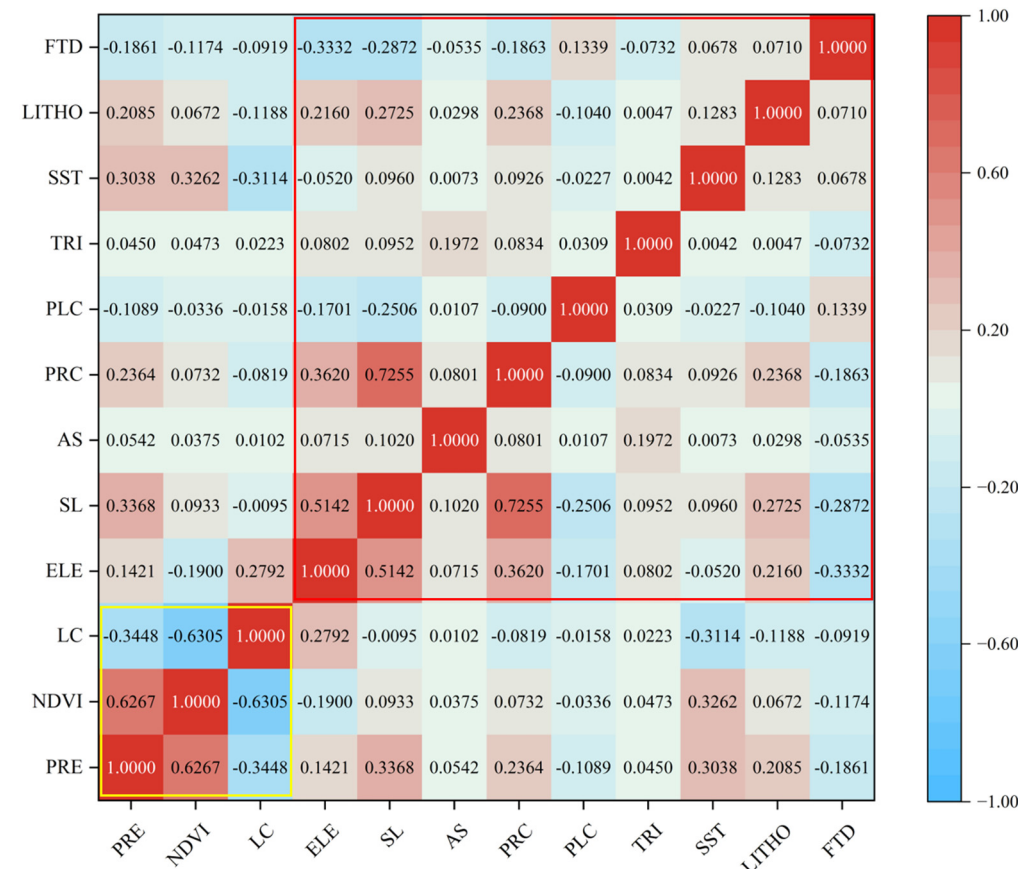


Figure 5. The *PCC* calculation results of condition factors. (Areas in the red box represent correlations between static factors, areas in the yellow box represent correlations between dynamic factors, and other areas represent correlations between dynamic and static factors.)

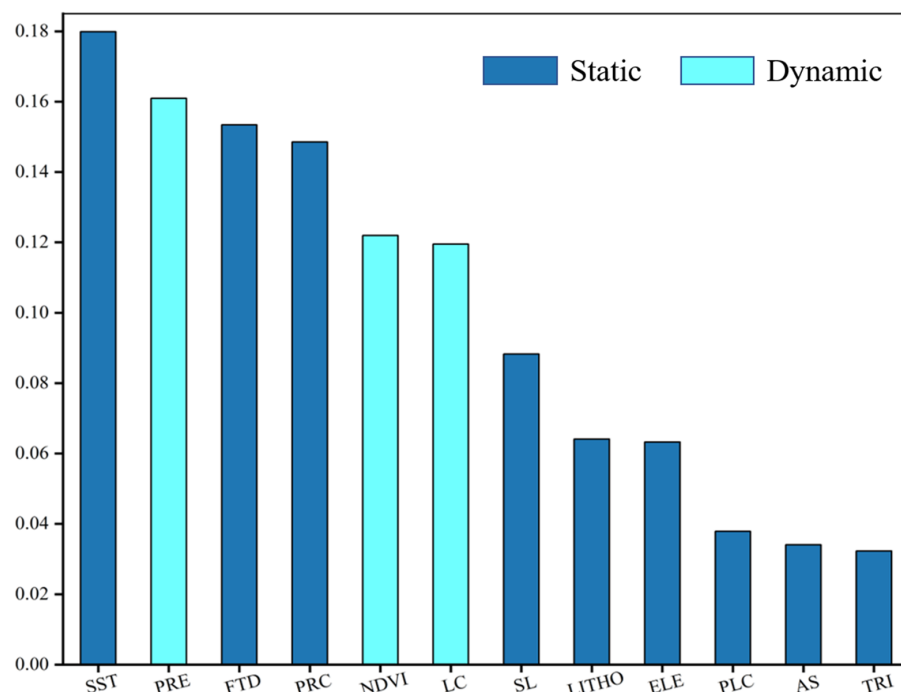


Figure 6. The *MI* calculation results of condition factors.

Based on these factor selection results, we further analyzed the interactions between static and dynamic factors to better understand their combined impact on landslide susceptibility. As demonstrated in Figure 5, the red-highlighted areas signify the correlation between static factors, while the yellow-highlighted areas denote the correlation between dynamic factors. The remaining areas indicate the correlation between dynamic factors and static factors. Elevation, slope, and profile curvature exhibit strong correlations, indicating that these topographic static factors collectively influence the geomorphological stability of the slope. Furthermore, precipitation and land cover demonstrate a discernible pattern of correlation, indicating their role as dynamic factors that vary with time and season. It is noteworthy that precipitation exhibits a negative correlation with certain static factors (e.g., plane curvature and distance to faults), suggesting that precipitation-driven landslides may be more prevalent in low-curvature and gently sloping areas due to moisture accumulation. As demonstrated in Figure 6, the *MI* results illustrate the relative importance of various factors influencing landslide susceptibility. Among the static factors, surface soil type, elevation, and distance to faults exhibit high *MI* values, underscoring their fundamental role in landslide occurrence. Among the dynamic factors, precipitation and land cover demonstrate significant *MI* values, emphasizing their direct influence in triggering slope failure. The comparison of *MI* values between static and dynamic factors suggests that, while static factors primarily determine the baseline susceptibility of an area, dynamic factors such as precipitation act as key triggers, especially in areas that are already susceptible to instability. Therefore, landslide susceptibility is the result of a combination of long-term static topographic features and short-term dynamic environmental conditions.

4.1.2. Analysis of Dynamic Factor Changes in China from 2001 to 2022

We used ArcGIS 10.8 software to generate spatial distribution maps of precipitation, NDVI, and land cover type in China from 2001 to 2022 and tested the trends (Figure 7). The results showed that between 2001 and 2022, precipitation reached a maximum of 13,463.5 mm and a minimum of 2.95 mm. Overall, south-central China received more precipitation each year, with the highest amounts in southern Tibet and lower amounts in northwest China (Figure 7a). During these 22 years, there was no significant trend in precipitation

in most regions of China. This stability suggests that the use of annual precipitation data remains a valid method for assessing long-term landslide susceptibility trends. However, a few regions, such as northern Xinjiang, central Henan, parts of Yunnan, and Taiwan, exhibited a significant decreasing trend in precipitation ($p < 0.05$), while some areas, including southwestern Xizang, Heilongjiang, the border regions of Inner Mongolia and Jilin, northeastern Zhejiang, and parts of Qinghai, showed a significant increasing trend ($p < 0.05$) (Figure 7b). The NDVI showed a clear north–south divide, with the Heihe–Tengchong line as the boundary and a lower NDVI in the north and a higher NDVI in the south. This could be because the southern region, with more precipitation and dense vegetation, had a higher NDVI than the northern region, which had less precipitation and sparse vegetation (Figure 7c). Over 22 years, the NDVI increased significantly ($p < 0.01$) in most regions of China, while it decreased significantly in few regions (Figure 7d). The predominant land cover type in China's northern and northwestern region is non-vegetative, with shrub and grassland ecosystems dominating the central regions, and a variety of tree-based and other vegetative cover types dominating the south. Cities, buildings, water bodies, permanent snow, and ice were sparsely distributed (Figure 7e). During the 22-year observation period, China's rapid economic development caused significant changes in land cover types across the country. These changes indicate a gradual expansion of land use and a discernible trend towards the transition between different land cover types. Regions without noticeable change trends, however, were primarily characterized by distinct topographic features that rendered them difficult to utilize. These include deserts and wastelands in non-vegetated areas, alpine forests in vegetated regions, and construction land that has already been used (Figure 7f).

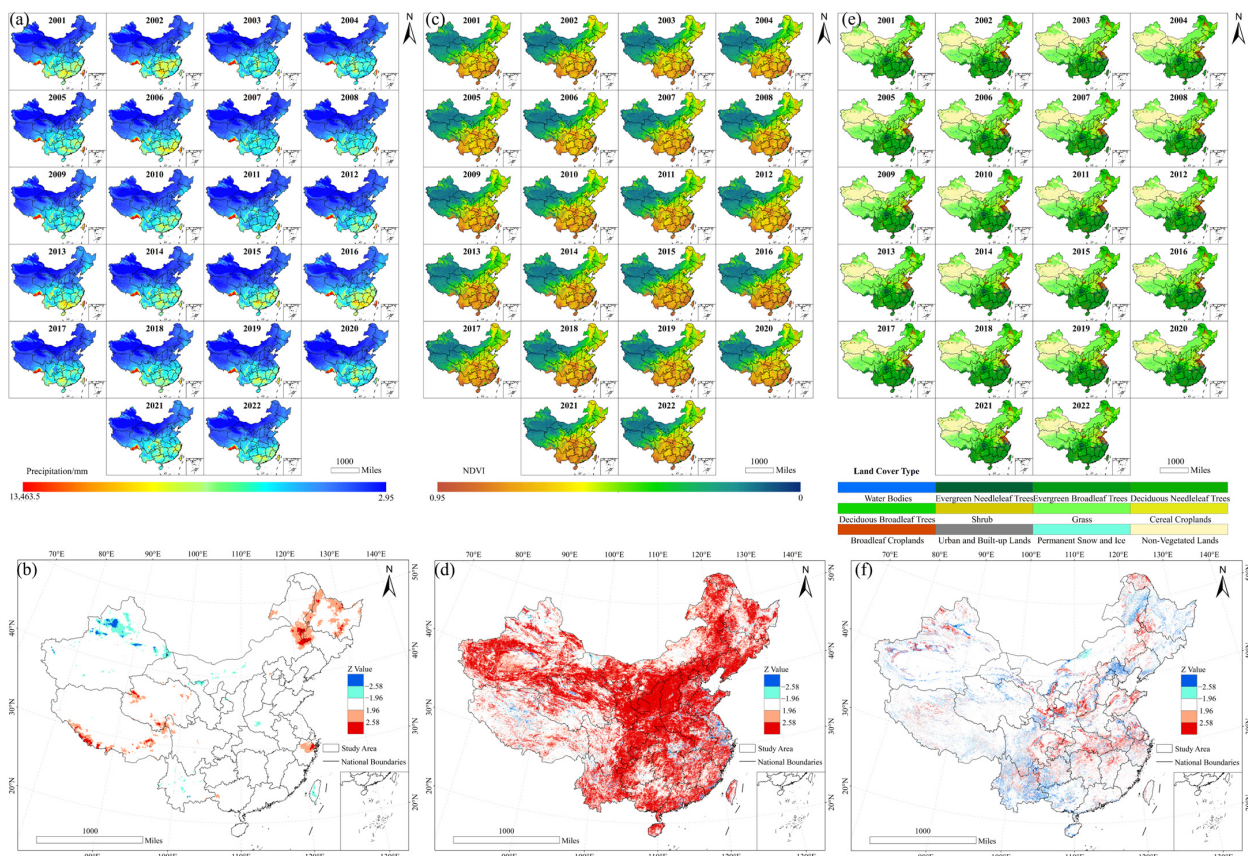


Figure 7. Spatial distribution of precipitation, NDVI, and land cover types (a,c,e) and their change trends test (b,d,f) during 2001–2022.

4.2. Model Evaluation Results

The metrics of f1-measure, recall, and accuracy for the three models were derived from a confusion matrix applied to the test dataset following the training phase. Additionally, the model performance was evaluated using AUC values (Figure 8). The ROC for the SVM, CNN, and ResNet18 models yielded AUC values of 0.9209, 0.9322, and 0.9362, respectively. All exceeded the threshold of 0.9, indicating that these models exhibited an excellent test performance on this dataset. The test data exhibited accuracies of 0.8489, 0.862, and 0.862, recalls of 0.7282, 0.8106, and 0.8788, and f1-measures of 0.7672, 0.7962, and 0.809 for the respective models. The findings demonstrate that the ResNet18 model achieves optimum performance in predicting the probability of landslide susceptibility.

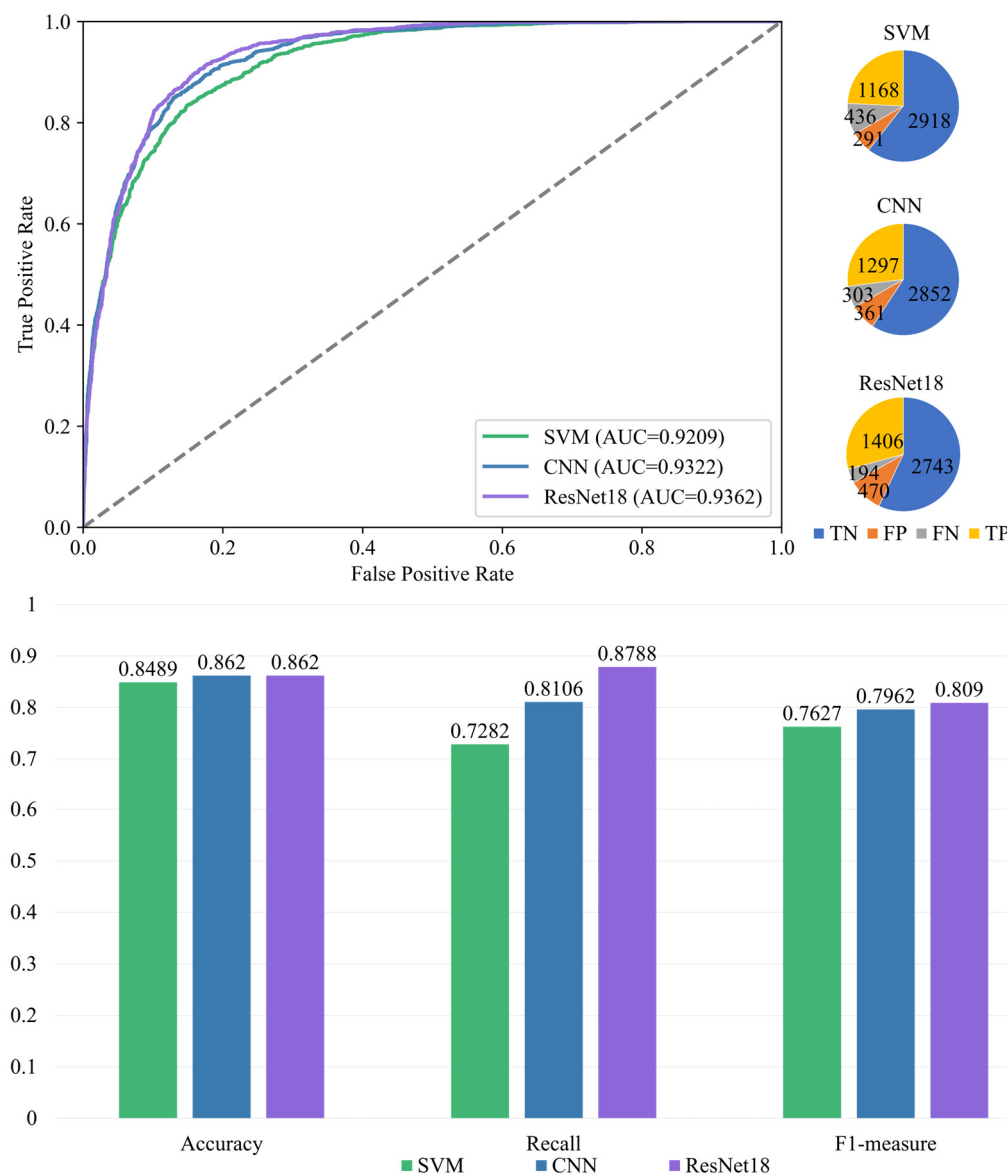


Figure 8. ROC curve and accuracy evaluation of test data.

4.3. Dynamic Evaluation of Landslide Susceptibility and Temporal Probability Analysis of Typical Regions in China

4.3.1. Dynamic Evaluation Results and Analysis of Large-Scale Landslide Susceptibility Trends in China from 2001 to 2022

Using the trained model, we evaluated the probability of landslide events occurring from 2001 to 2022 and generated a dynamic large-scale landslide susceptibility map for

22 years. The equal-interval classification technique was employed to categorize susceptibility probabilities into five distinct levels: extremely high (0.8–1), high (0.6–0.8), medium (0.4–0.6), low (0.2–0.4), and extremely low (0–0.2). The area percentage for each landslide susceptibility subzone was calculated for each year (Figure 9). The MK test was conducted on the forecast probability map (Figure 10). The results showed that regions with high and extremely high landslide susceptibility in China were predominantly located in southern Xizang, Yunnan, Guizhou, Sichuan, Chongqing, Hunan, southern Gansu, Shaanxi, Shanxi, western Hebei, western Henan, Hubei, Anhui, Shanghai, Zhejiang, Guangxi, Guangdong, Hainan, Taiwan, on the southeastern coast of Jiangsu, and in the areas along the Tien Shan, Kunlun Mountains, and Qilian Mountains in northern China (Figure 10a). The combined area percentages for high and extremely high susceptibility were recorded at 10.22 percent and 12.97 percent, respectively. Except for a few areas with low precipitation, most areas had high precipitation. Overall, the spatial distribution of landslide susceptibility zones closely correlated with precipitation patterns, as regions with elevated precipitation demonstrated a higher likelihood of landslide occurrences. From the spatial trend test, the probability of landslide susceptibility in the regions of southern Xizang, eastern Sichuan, western Chongqing, the Sichuan–Guizhou border, Heilongjiang, northern Inner Mongolia, and coastal Liaoning, northern Gansu, northern Shanxi, central and western Xinjiang, coastal Guangdong, central Zhejiang, coastal Shandong, central Hunan, southern Anhui, south-central Guangxi, north-central Jiangxi, north-central Qinghai, and along the border of Inner Mongolia and Jilin showed a significant increasing trend ($p < 0.01$). In contrast, the landslide susceptibility at the border of Gansu and Ningxia and in north-central Shaanxi, northern Shanxi, western Henan, northern Hebei, southern Fujian, and south-central Yunnan showed a significant decreasing trend ($p < 0.01$) (Figure 10b). Based on the spatial distribution and variation trend of landslide susceptibility, the probability of landslide occurrence in southeastern Xizang, along the border of the Sichuan, Chongqing, and Guizhou provinces, along the coast of Guangdong, on the northern coast of Shandong, and in central Zhejiang, southern Anhui, central Hunan, central Jiangxi, central and southern Guangxi, and Hong Kong was high and showed a significant increasing trend ($p < 0.01$). The probability of landslide occurrence in southern Gansu, north-central Shaanxi, South Shanxi, west Henan, central Yunnan, south Fujian, Hainan, and Taiwan was high and showed a significant decreasing trend ($p < 0.01$).

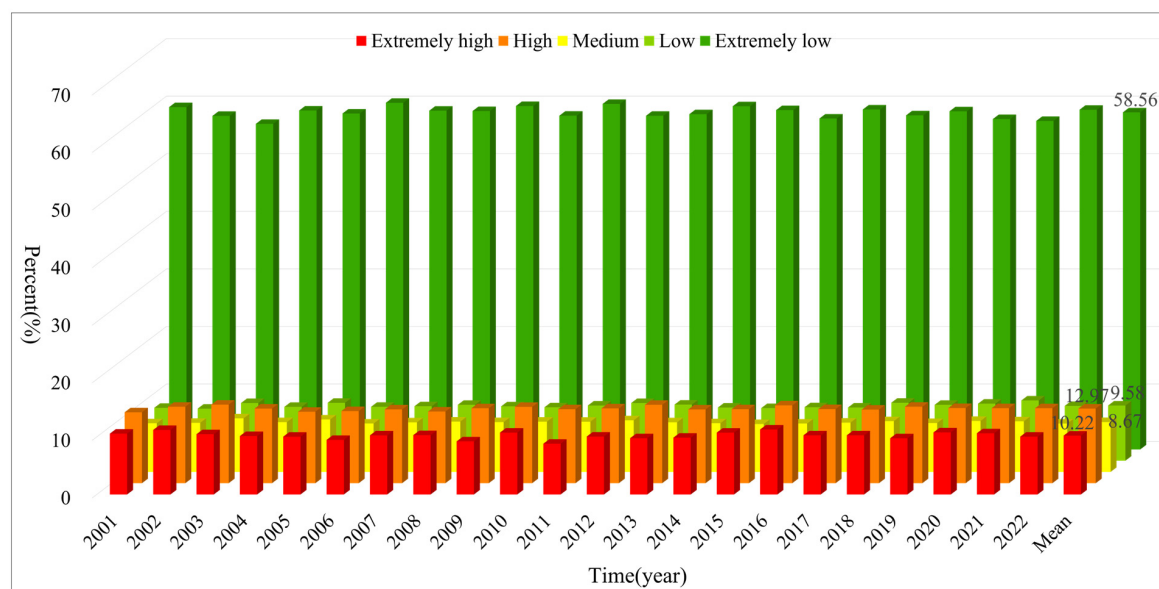


Figure 9. Percentage area distribution of landslide susceptibility zones from 2001 to 2022.

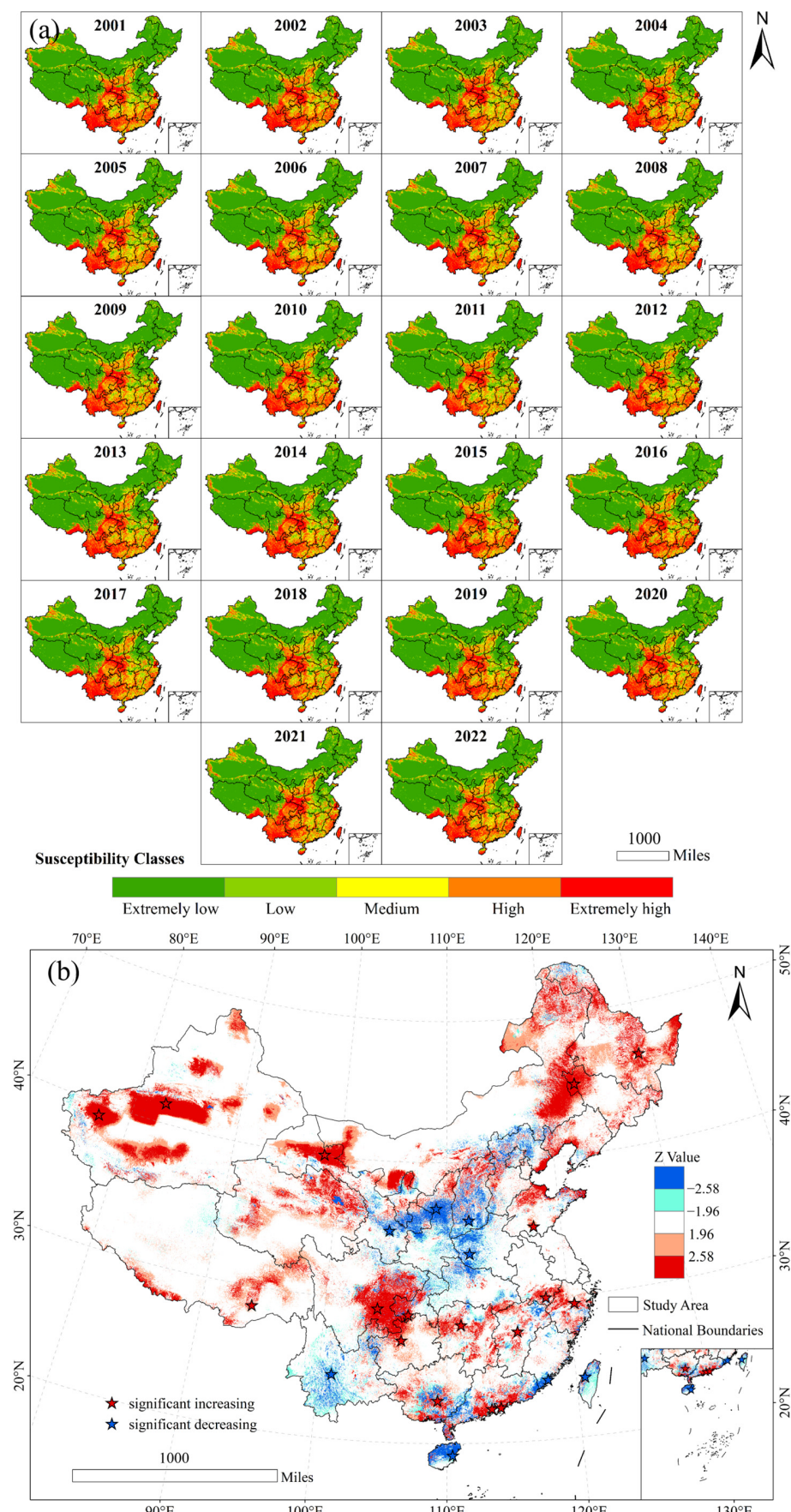


Figure 10. Spatial distribution of LSM (a) and spatial change trend test landslide susceptibility (b) from 2001 to 2022.

4.3.2. Temporal Analysis Results of Large-Scale Landslide Susceptibility in Typical Area

Figure 11 depicts the results of the one-dimensional linear regression method to fit typical regions linearly. Twelve regions with a high probability of landslide occurrence and significantly increasing trends were chosen: Anhui, Chongqing, Guangdong, Guangxi, Guizhou, Hunan, Jiangxi, Shandong, Sichuan, Hong Kong, Xizang, and Zhejiang (Figure 10b partial red pentagram region). In addition, eight regions with a high probability of landslide occurrence and significantly decreasing trends, Fujian, Gansu, Hainan, Henan, Shaanxi, Shanxi, Taiwan, and Yunnan (Figure 10b, blue pentagram region), were randomly selected, with a total of 20 regional points. The fitting results for Anhui, Chongqing, Guangdong, Guangxi, Guizhou, Hunan, Jiangxi, Shandong, Sichuan, Hong Kong, Xizang, and Zhejiang show a general upward trend at these regional points from 2001 to 2022. There were two clear turning points in 2005 and 2012, when the probability of landslides occurring in these two years was lower than that in the other years. Furthermore, special attention should be paid to Chongqing, Guizhou, and Sichuan, which are three areas prone to landslide disasters, where the probability of landslide occurrence increased by more than 10 percentage points between 2001 to 2022. Conversely, the fitting results for Fujian, Gansu, Hainan, Henan, Shaanxi, Shanxi, Taiwan, and Yunnan demonstrated a general decline in the probability of landslides in these regions between 2001 and 2022. Notably, five regions, Fujian, Gansu, Hainan, Henan, and Taiwan, exhibited minimal declines in landslide susceptibility. In comparison, two regions, Shaanxi and Shanxi, experienced a notable decrease in landslide probability of over 10 percentage points.

4.4. Results of Conditioning Factor Interpretability Analysis Based on the SHAP

To clarify the influence of different conditioning factors on landslide evaluation modeling in DL models and enhance the model's explanatory capacity, we adopted the SHAP methodology. We calculated the SHAP value of the ResNet18 model, and the results are presented in Figure 12. The results revealed that precipitation had the greatest influence on model training, followed by profile curvature, NDVI, distance to faults, and land cover type (Figure 12a). As depicted in Figure 12b, the eigenvalues on the right side of the graph, represented in red to signify high precipitation levels, exhibited a positive correlation with the SHAP values, while the side indicates contributions to the likelihood of landslide events. This suggests that increased precipitation correlates with a heightened probability of landslides. Analyses of LCFs and the results of our spatial analysis show a positive correlation between landslide distribution in China and precipitation levels, corroborating the findings derived from Shapley value calculations.

Furthermore, to investigate the interactions between dynamic and static factors in influencing landslide susceptibility, we examined the combined effects of precipitation, NDVI, and land cover with key static factors such as aspect, elevation, and distance to faults. The SHAP results indicate that while precipitation is the most dominant factor, its influence is significantly modulated by topographic and geological conditions. For example, areas with high precipitation and steep slopes exhibit a markedly higher probability of landslides, suggesting a coupling effect between dynamic and static variables. Similarly, regions with dense vegetation (high NDVI) tend to exhibit reduced landslide susceptibility, but this mitigating effect weakens in areas with fragile lithology or near fault zones. These findings align with the results presented in Figure 6, which illustrates the MI values for both static and dynamic factors. The MI analysis confirms that precipitation, NDVI, and land cover are among the most influential dynamic variables, while static factors such as surface soil taxonomy, lithology, and distance to faults also play a critical role in determining landslide susceptibility.

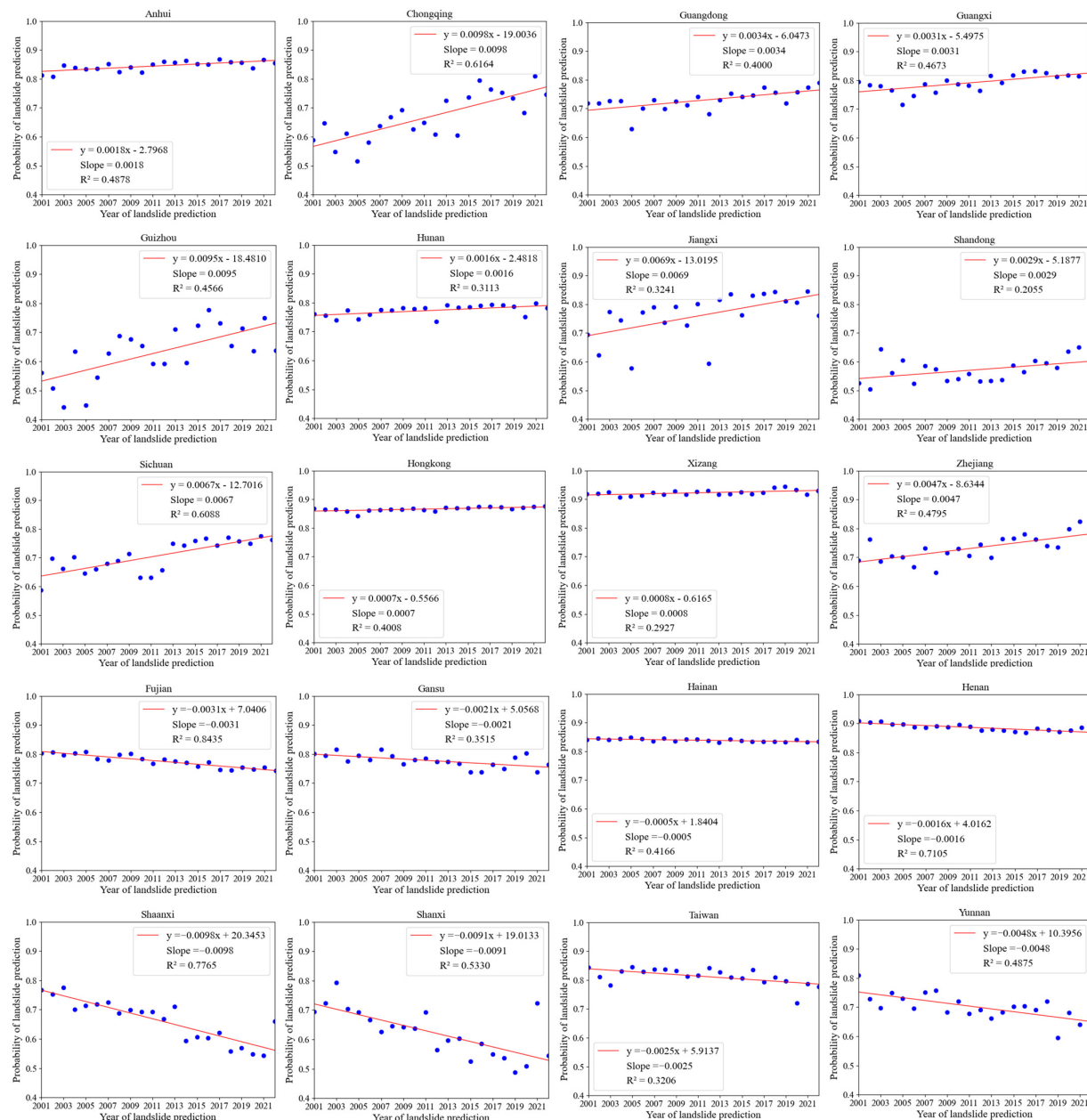


Figure 11. Temporal of landslide susceptibility in typical regions of China, 2001–2022 (red solid line is linear regression, the blue circle is the predicted probability of landslide in the corresponding year).

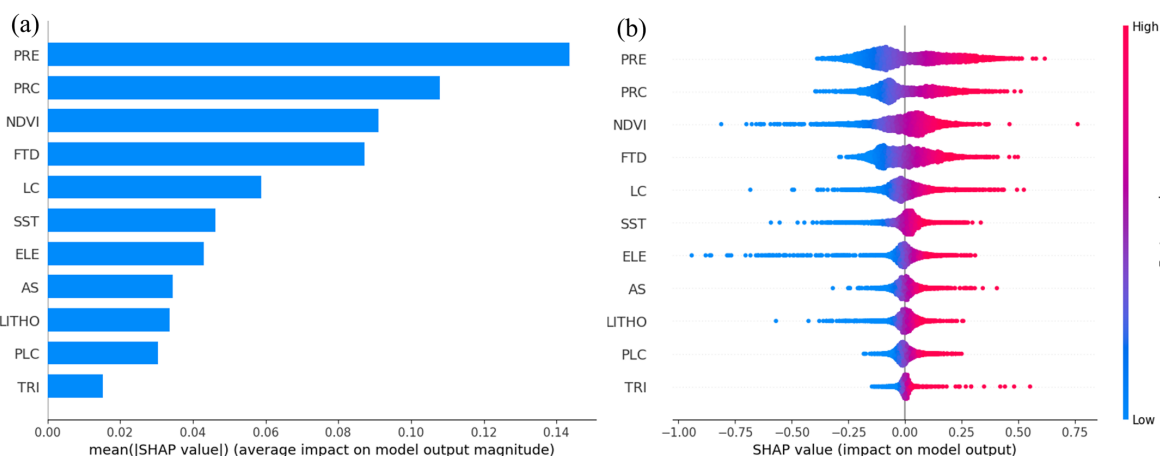


Figure 12. Ranking of feature importance based on SHAP method (a) and summary plot (b).

5. Discussion

5.1. Global Training vs. Local Training

The study employed global training data to model large-scale landslide susceptibility in China. To validate the model's robustness, it was trained on local training data, and both the global and local models were subsequently evaluated using local testing data. The results of these tests are illustrated in Figure 13. The findings indicate that the SVM and CNN models trained on local data outperform those trained on global data; however, the opposite is true for the ResNet18 model. This demonstrates that when only a few samples are available, the CNN has a relatively simple structure with fewer parameters and can be trained more efficiently. The SVM is better at handling high-dimensional data and generalizing small-sample data. The ResNet18 architecture is inherently deeper than traditional CNNs, and as the dataset size increases, the advantages of its deeper structure become more pronounced. Specifically, ResNet18 outperforms CNNs in terms of predictive accuracy when trained on large volumes of data. In addition, the results of the testing model on the local areas of the global training models showed that ResNet18 exhibited the best robustness. Regarding the recall and f1-measure metrics, the ResNet18 model utilizing global training data achieved the best performance. Consequently, this study provides a sound and reliable framework for evaluating landslide susceptibility in China, employing the ResNet18 model with global training data.

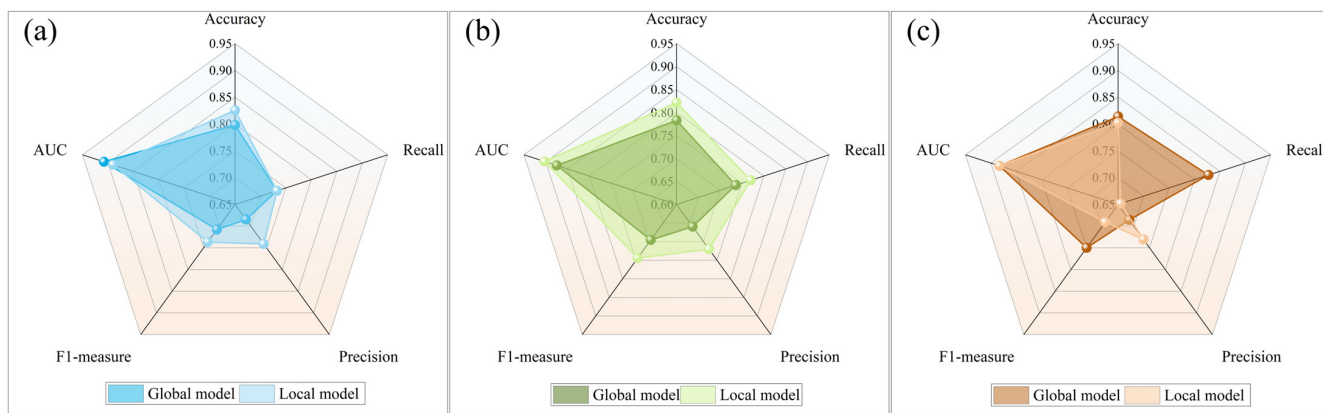


Figure 13. Test and comparison of local datasets across various models: (a) SVM, (b) CNN, and (c) ResNet18.

Additionally, this study undertook an examination of the performance of the SVM, CNN, and ResNet18 models, focusing on metrics such as parameters, training time, and f1-measure in the global and local training landslide susceptibility assessments, as shown in Table 4. SVMs and CNNs are known to be efficient and practical choices when the sample size is limited. Conversely, when data resources are ample, ResNet18 is capable of delivering a more precise and robust evaluation of landslide susceptibility. Therefore, landslide susceptibility evaluation models should be selected based on specific application scenarios and data sizes. Based on the ResNet18 model, this study used global training data to assess the landslide susceptibility of China, which not only reflected the advantages of the DL model in processing large-scale data but also provided strong technical support for large-scale landslide assessment in the future. By using this approach, decision makers can be provided with a strong, data-driven basis that can make a significant contribution to improving environmental and regional policy. It also provides important evidence for landslide disaster warning, prevention and mitigation, ensuring that proactive measures are consistent with regional planning and environmental management objectives.

Table 4. SVM, CNN, and ResNet18 models in global training versus local training comparison.

Model	Hyperparameter or Network Parameter	Training Time ¹ (Relative)	F1-Measure (Global Training)	F1-Measure (Local Training)
SVM	2	0.28 h	0.762	0.736
CNN	67,171,009	1.85 h	0.796	0.744
ResNet18	11,529,729	1.25 h	0.809	0.691

Notes: The f1-measure represents the f1-measure obtained from testing the global and local training data. ¹ Experimental environment: framework—TensorFlow2.10 + cuda11.8, CPU—Intel (R) Core (TM) i5-13400F, GPU—GeForce RTX 4080 (16 G).

In addition to the comparison between the SVM, CNN, and ResNet18 models, it is important to consider the computational trade-offs associated with the ResNet18 model, especially in the context of large-scale landslide susceptibility assessments. Table 4 presents a comparative analysis of key factors, including the training time and f1-measure for both global and local training. While ResNet18 shows superior performance in terms of delivering more precise and robust results, as indicated by its higher f1-measure for global training (0.809), its longer training time (1.25 h) is a key consideration. This factor must be taken into account when deploying this model in real-world scenarios. Despite the increased training time, ResNet18's deep learning architecture offers significant scalability advantages, particularly for large-scale applications. The model's ability to handle vast datasets, such as the global landslide data used to assess landslide susceptibility in China, makes it highly suitable for large-scale, real-time landslide risk assessment tasks. In practical terms, while the training process may be more resource-intensive, once the model is trained, it can efficiently process large amounts of data. This ensures fast and scalable predictions for landslide susceptibility across broad geographical areas. Moreover, with advancements in computational power and parallel processing techniques, the time required for training models like ResNet18 can be reduced significantly. Thus, the initial computational expense is offset by the long-term benefits in terms of model robustness, accuracy, and the ability to handle large datasets efficiently. These factors make ResNet18 a highly promising tool for large-scale landslide assessment applications, where high accuracy and scalability are crucial.

5.2. Comparison of Evaluation Results of Landslide Susceptibility

Based on the global dynamic landslide susceptibility model, the large-scale landslide susceptibility in China from 2001 to 2022 has been evaluated and its spatial variation trends analyzed. The results indicate that regions with high and extremely high landslide susceptibility are predominantly concentrated in southwest China. A comparative analysis of the landslide susceptibility zones produced in this study with those from two existing national assessments reveals both similarities and differences (Figure 14). Liu [29] suggested that the spatial distribution of landslide risk in China is largely delineated by the Heihe-Tengchong line, with the western regions characterized by predominantly low-risk areas, and the eastern regions exhibiting higher concentrations of medium to high-risk zones (Figure 14a). Similarly, Wang [31] identified areas of high landslide risk in southwest China, as well as in the hilly regions south of the Yangtze River (Figure 14b). In general, the spatial distribution of landslide susceptibility in this study (Figure 14c,d) aligns well with previous assessments (Figure 14a,b), though some regional differences are evident. For instance, Liu [29] categorized the southern Gansu region and the border area between Chongqing and Sichuan as medium- to high-risk zones, whereas this study classifies these areas as very high-risk. Similarly, Wang [31] identified Hunan, Jiangxi, and other regions as areas of extreme susceptibility, a finding that is consistent with the results of this study. These

discrepancies can likely be attributed to differences in the landslide databases used in each study, which may lead to variations in the identification of landslide-prone areas due to differences in the regional distribution of landslide events.

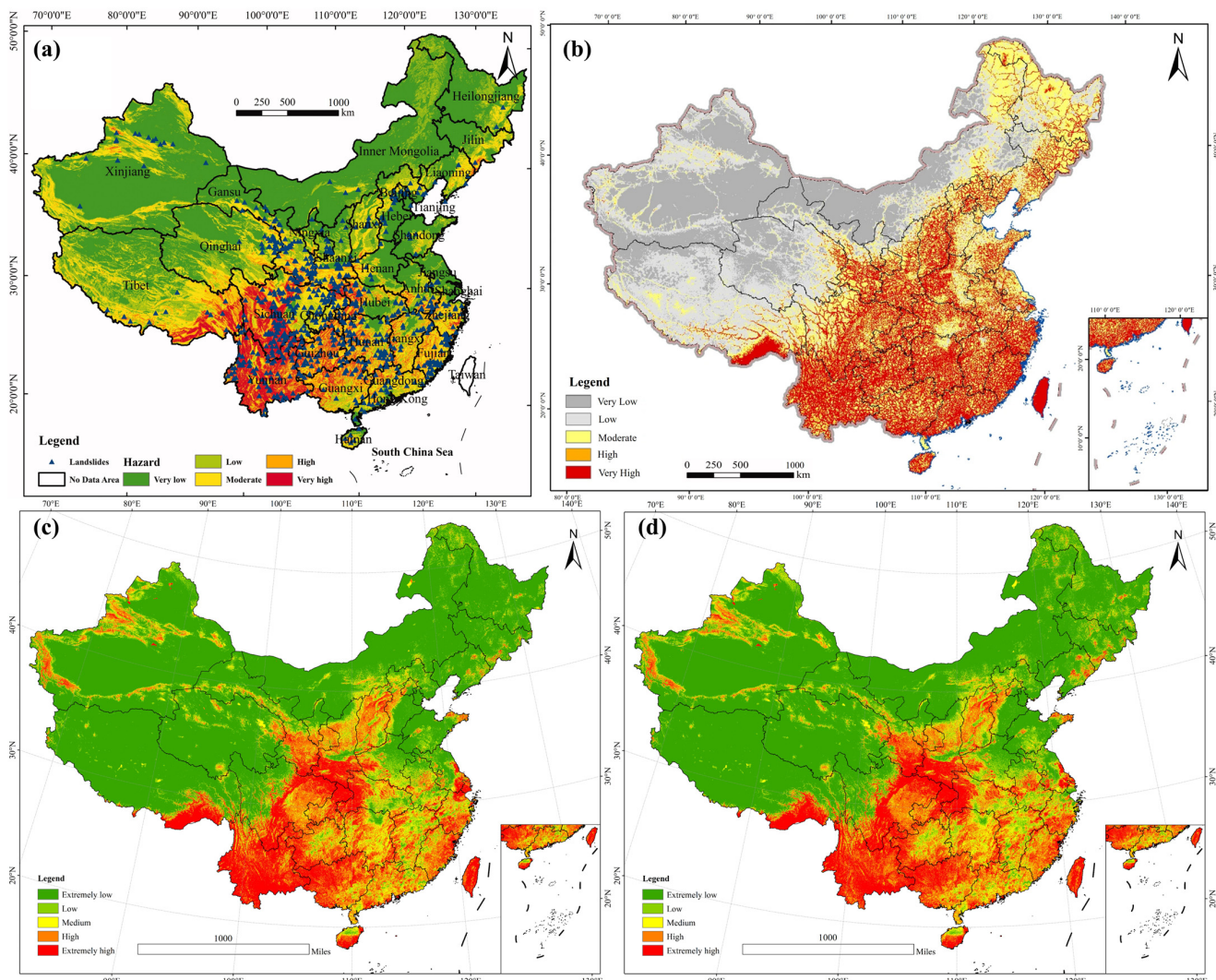


Figure 14. Comparison analysis of landslide susceptibility maps from previous studies. (a) Landslide hazard map developed by Liu [29]. (b) LSM prepared by Wang [31]. (c) LSM for 2017 based on the ResNet18 from this study. (d) LSM for 2020 based on the ResNet18 from this study.

Additionally, a trend analysis of large-scale landslide susceptibility in China over the past 22 years reveals a significant increase in susceptibility in certain regions, particularly in Chongqing, Guizhou, and Sichuan, where the probability of landslide occurrence has notably risen. Lin and Wang [65] conducted a time-series analysis of China's recorded catastrophic landslides, showing a clear upward trend in the frequency of such events. Liu [29] also mentioned an increase in landslide risk in China over the next decade, with high-risk areas expected to expand westward beyond the Heihe–Tengchong line. At the same time, Zhang and Ding [66] study showed that the areas in Sichuan with high and extremely high landslide susceptibility have increased with the increase in rainfall in recent decades. Therefore, the large-scale landslide occurrence in some areas of China has shown an obvious increasing trend in the past 20 years, and the landslide trend in Sichuan and other places, especially, should be paid attention.

5.3. Analysis of Limitations

Although this study achieved significant results, it has some limitations. First, the inherent bias in the underlying landslide data and possible incompleteness of the single global landslide database used in this study may have impacted the landslide evaluation. At the same time, this study reflects only the trend of large-scale landslides in large regions, and further research is needed on the trend of small regional landslides. In terms of dataset biases, while we used a global landslide database, it is important to acknowledge the inherent limitations and biases that may arise from the database itself. These include the potential underreporting of landslides in certain regions, the reliance on historical landslide records, which may miss recent events, and variations in reporting standards across different countries and regions. Such biases could impact the accuracy and representativeness of the landslide data, particularly in areas with sparse data or where landslides are not systematically recorded.

Second, uncertainties and limitations exist in the selected LCFs. Although DEMs nowadays are highly accurate, this study employed a spatial resolution of 1 km, which resulted in some small slopes not being reflected, thereby affecting the landslide evaluation.

Third, the main objective of this study is to assess landslide susceptibility on a large scale and in the long term. However, some landslides are triggered by extreme events (e.g., rainfall). In order to smooth out the effects of short-term extreme events and to avoid single extreme events causing frequent local landslides and, thus, affecting the overall trend analysis, an annual temporal resolution is used in this paper. In addition, the annual temporal resolution is more appropriate for the analytical framework of this study, given the time span of the data. Therefore, the annual scale trend analysis in this paper does not further investigate the specific impact of extreme events on large-scale landslide hazard susceptibility. Existing studies [19,25] have shown that the impact of short-term extreme rainfall events on landslides can be more accurately captured using data with a higher temporal resolution. Therefore, future studies should consider introducing finer temporal resolution data to gain a deeper understanding of the interaction between short-term extreme weather events and landslides.

This study used interpretable techniques to conduct an in-depth analysis of the DL models, revealing the crucial role of precipitation in landslide occurrence. Although SHAP was used to explain the model, the results were not fed back into the variable selection process to demonstrate the benefits of SHAP. In light of the limitations identified in this study, future research should focus on refining data collection by integrating more localized, real-time, and high-resolution datasets to overcome biases and improve the representativeness of landslide data. Additionally, selecting a broader range of dynamic factors and employing higher temporal resolutions, such as monthly or daily records, would allow for more accurate modeling of landslide susceptibility, especially in areas with rapid environmental changes. Enhancing model interpretation techniques, such as incorporating real-time monitoring systems and advanced machine learning methods, will further improve the precision and reliability of landslide predictions. This will ultimately strengthen the overall dependability of susceptibility assessments.

6. Conclusions

In the study, we constructed a global dynamic landslide susceptibility model employing ResNet18. By combining this with the GEE platform, we obtained spatial distribution data for the dynamic conditioning factors in the Chinese region from 2001 to 2022. We then employed the SHAP method to elucidate the effect of the input features on the output results generated by the ResNet18 model, thereby highlighting the influence of LCFs on the model. Finally, this study assessed large-scale landslide susceptibility in China from 2001 to

2022 and used the MK test to examine spatial trend changes in landslide susceptibility over 22 years. A time-series analysis of large-scale landslide susceptibility in typical Chinese regions was carried out. The principal findings are summarized as follows.

1. Testing the spatial distribution of precipitation, NDVI, and land cover type in China from 2001 to 2022 revealed that precipitation did not show any significant spatial change trends over the 22-year period. In contrast, the NDVI exhibited a significant increasing trend, while the changes in land-cover types were complex and diverse.
2. In the model performance evaluation, the SVM, CNN, and ResNet18 models demonstrated excellent performance ($AUC > 0.9$), with the ResNet18 model outperforming the others with an AUC of 0.9362.
3. The findings from the SHAP analysis demonstrate that precipitation is the most influential factor affecting landslides, exhibiting a substantial positive spatial correlation with the likelihood of landslide events. Subsequently, other factors, including profile curvature, NDVI, and distance to faults, exert a pronounced influence on landslide occurrence.
4. Based on the spatial distribution of LSM evaluated in China from 2001 to 2022 and statistics on the area share of large-scale landslide susceptibility, research indicates that the zones in China exhibiting high and extremely high susceptibility to landslides are predominantly located in the southwest regions of the country. Over a span of 22 years, the average area shares of the high and extremely high landslide susceptibility zones were recorded at 12.97 percent and 10.22 percent, respectively. Furthermore, the spatial trend test of large-scale landslide susceptibility and the time series analysis of typical regional points indicate that the areas with high landslide susceptibility in Chongqing, Guizhou, and Sichuan have a significant increasing trend, with landslide susceptibility increasing by more than 10 percentage points over 22 years. In contrast, the areas with high landslide susceptibility in Shaanxi and Shanxi showed a significant decreasing trend, with landslide susceptibility decreasing by more than 10 percentage points over 22 years. These findings may provide a valuable reference for subsequent investigations into landslide hazards in China.

Author Contributions: Conceptualization, H.J., M.D. and W.H.; methodology, H.J., M.D. and W.H.; software, H.J.; validation, H.J. and W.H.; formal analysis, H.J. and M.D.; investigation, L.L.; resources, M.D. and L.L.; data curation, H.J. and L.L.; writing—original draft, H.J.; writing—review and editing, M.D. and W.H.; visualization, H.J. and W.H.; supervision, L.L.; project administration, M.D.; funding acquisition, M.D. All authors have read and agreed to the published version of the manuscript.

Funding: This work was partly supported by the National Natural Science Foundation of China under Grants 42374027; the Shaanxi Province Geoscience Big Data and Geohazard Prevention Innovation Team (2022); the Opening Fund of Key Laboratory of Smart Earth under Grant KF2023YB04-01; the Key R&D Program Projects in Zhejiang Province under Grant 2023C03177.

Institutional Review Board Statement: Not applicable.

Informed Consent Statement: Not applicable.

Data Availability Statement: The article provides a comprehensive description of all data sources utilized in the study. Interested parties may request access to the established dynamic model of landslide susceptibility mapping by contacting the corresponding author via email.

Acknowledgments: The authors are grateful to the editor of the journal and the anonymous reviewers for their valuable comments and recommendations. Thanks to Chang'an University High Performance Computing Platform.

Conflicts of Interest: The authors declare no conflicts of interest.

References

1. Petley, D. Global patterns of loss of life from landslides. *Geology* **2012**, *40*, 927–930. [[CrossRef](#)]
2. Haque, U.; Blum, P.; Da Silva, P.F.; Andersen, P.; Pilz, J.; Chalov, S.R.; Malet, J.-P.; Auflieč, M.J.; Andres, N.; Poyiadji, E. Fatal landslides in Europe. *Landslides* **2016**, *13*, 1545–1554. [[CrossRef](#)]
3. Yilmaz, I. Comparison of landslide susceptibility mapping methodologies for Koyulhisar, Turkey: Conditional probability, logistic regression, artificial neural networks, and support vector machine. *Environ. Earth Sci.* **2010**, *61*, 821–836. [[CrossRef](#)]
4. Yang, X.; Liu, R.; Yang, M.; Chen, J.; Liu, T.; Yang, Y.; Chen, W.; Wang, Y. Incorporating landslide spatial information and correlated features among conditioning factors for landslide susceptibility mapping. *Remote Sens.* **2021**, *13*, 2166. [[CrossRef](#)]
5. Li, L.; Lan, H. Bivariate landslide susceptibility analysis: Clarification, optimization, open software, and preliminary comparison. *Remote Sens.* **2023**, *15*, 1418. [[CrossRef](#)]
6. Froude, M.J.; Petley, D.N. Global fatal landslide occurrence from 2004 to 2016. *Nat. Hazards Earth Syst. Sci.* **2018**, *18*, 2161–2181. [[CrossRef](#)]
7. Lan, H.; Zhou, C.; Wang, L.; Zhang, H.; Li, R. Landslide hazard spatial analysis and prediction using GIS in the Xiaojiang watershed, Yunnan, China. *Eng. Geol.* **2004**, *76*, 109–128. [[CrossRef](#)]
8. Li, L.; Lan, H.; Guo, C.; Zhang, Y.; Li, Q.; Wu, Y. A modified frequency ratio method for landslide susceptibility assessment. *Landslides* **2017**, *14*, 727–741. [[CrossRef](#)]
9. Huang, W.B.; Ding, M.T.; Li, Z.H.; Yu, J.C.; Ge, D.Q.; Liu, Q.; Yang, J. Landslide susceptibility mapping and dynamic response along the Sichuan-Tibet transportation corridor using deep learning algorithms. *CATENA* **2023**, *222*, 106866. [[CrossRef](#)]
10. Hakim, W.L.; Rezaie, F.; Nur, A.S.; Panahi, M.; Khosravi, K.; Lee, C.-W.; Lee, S. Convolutional neural network (CNN) with meta-heuristic optimization algorithms for landslide susceptibility mapping in Icheon, South Korea. *J. Environ. Manag.* **2022**, *305*, 114367. [[CrossRef](#)] [[PubMed](#)]
11. Ge, Y.; Liu, G.; Tang, H.; Zhao, B.; Xiong, C. Comparative analysis of five convolutional neural networks for landslide susceptibility assessment. *Bull. Eng. Geol. Environ.* **2023**, *82*, 377. [[CrossRef](#)]
12. Yu, L.; Wang, Y.; Pradhan, B. Enhancing landslide susceptibility mapping incorporating landslide typology via stacking ensemble machine learning in Three Gorges Reservoir, China. *Geosci. Front.* **2024**, *15*, 101802. [[CrossRef](#)]
13. He, K.; Zhang, X.; Ren, S.; Sun, J. Deep residual learning for image recognition. In Proceedings of the IEEE Conference on Computer Vision and Pattern Recognition, Las Vegas, NV, USA, 27–30 June 2016; pp. 770–778.
14. Emberson, R.; Kirschbaum, D.; Stanley, T. Global connections between El Nino and landslide impacts. *Nat. Commun.* **2021**, *12*, 2262. [[CrossRef](#)] [[PubMed](#)]
15. Lin, Q.; Steger, S.; Pittore, M.; Zhang, J.; Wang, L.; Jiang, T.; Wang, Y. Evaluation of potential changes in landslide susceptibility and landslide occurrence frequency in China under climate change. *Sci. Total Environ.* **2022**, *850*, 158049. [[CrossRef](#)] [[PubMed](#)]
16. Lan, H.; Peng, J.; Zhu, Y.; Li, L.; Pan, B.; Huang, Q.; Li, J.; Zhang, Q. Research on geological and surficial processes and major disaster effects in the Yellow River Basin. *Sci. China Earth Sci.* **2022**, *65*, 234–256. [[CrossRef](#)]
17. Li, L.; Lan, H. Analytical ‘decisiveness’ as a robust measure of the absolute importance of landslide predisposing factors. *Int. J. Digit. Earth* **2024**, *17*, 2356161. [[CrossRef](#)]
18. Kirschbaum, D.B.; Stanley, T.; Simmons, J. A dynamic landslide hazard assessment system for Central America and Hispaniola. *Nat. Hazards Earth Syst. Sci.* **2015**, *15*, 2257–2272. [[CrossRef](#)]
19. Lee, J.-J.; Song, M.-S.; Yun, H.-S.; Yum, S.-G. Dynamic landslide susceptibility analysis that combines rainfall period, accumulated rainfall, and geospatial information. *Sci. Rep.* **2022**, *12*, 18429. [[CrossRef](#)] [[PubMed](#)]
20. Liu, Y.; Xu, P.; Cao, C.; Zhang, W.; Han, B.; Zhao, M. A quick method of early landslide identification based on dynamic susceptibility analysis using M-SVM method: A case study. *Bull. Eng. Geol. Environ.* **2023**, *82*, 454. [[CrossRef](#)]
21. Lin, X.; Xiao, G.; Zhou, H. Landslide susceptibility assessment method considering land use dynamic change. *J. Geoinf. Sci.* **2023**, *25*, 953–966.
22. Mondini, A.C.; Guzzetti, F.; Melillo, M. Deep learning forecast of rainfall-induced shallow landslides. *Nat. Commun.* **2023**, *14*, 2466. [[CrossRef](#)] [[PubMed](#)]
23. Distefano, P.; Peres, D.J.; Piciullo, L.; Palazzolo, N.; Scandura, P.; Cancelliere, A. Hydro-meteorological landslide triggering thresholds based on artificial neural networks using observed precipitation and ERA5-Land soil moisture. *Landslides* **2023**, *20*, 2725–2739. [[CrossRef](#)]
24. Nocentini, N.; Rosi, A.; Piciullo, L.; Liu, Z.; Segoni, S.; Fanti, R. Regional-scale spatiotemporal landslide probability assessment through machine learning and potential applications for operational warning systems: A case study in Kvam (Norway). *Landslides* **2024**, *21*, 2369–2387. [[CrossRef](#)]
25. Li, B.; Liu, K.; Wang, M.; He, Q.; Jiang, Z.; Zhu, W.; Qiao, N. Global dynamic rainfall-induced landslide susceptibility mapping using machine learning. *Remote Sens.* **2022**, *14*, 5795. [[CrossRef](#)]
26. Ahmed, M.; Tanyas, H.; Huser, R.; Dahal, A.; Titti, G.; Borgatti, L.; Francioni, M.; Lombardo, L. Dynamic rainfall-induced landslide susceptibility: A step towards a unified forecasting system. *Int. J. Appl. Earth Obs. Geoinf.* **2023**, *125*, 103593. [[CrossRef](#)]

27. Liu, C.; Li, W.; Wu, H.; Lu, P.; Sang, K.; Sun, W.; Chen, W.; Hong, Y.; Li, R. Susceptibility evaluation and mapping of China's landslides based on multi-source data. *Nat. Hazards* **2013**, *69*, 1477–1495. [[CrossRef](#)]
28. Stanley, T.; Kirschbaum, D.B. A heuristic approach to global landslide susceptibility mapping. *Nat. Hazards* **2017**, *87*, 145–164. [[CrossRef](#)] [[PubMed](#)]
29. Liu, X.; Miao, C. Large-scale assessment of landslide hazard, vulnerability and risk in China. *Geomat. Nat. Hazards Risk* **2018**, *9*, 1037–1052. [[CrossRef](#)]
30. Lin, Q.; Lima, P.; Steger, S.; Glade, T.; Jiang, T.; Zhang, J.; Liu, T.; Wang, Y. National-scale data-driven rainfall induced landslide susceptibility mapping for China by accounting for incomplete landslide data. *Geosci. Front.* **2021**, *12*, 101248. [[CrossRef](#)]
31. Wang, D.; Hao, M.; Chen, S.; Meng, Z.; Jiang, D.; Ding, F. Assessment of landslide susceptibility and risk factors in China. *Nat. Hazards* **2021**, *108*, 3045–3059. [[CrossRef](#)]
32. Juang, C.S.; Stanley, T.A.; Kirschbaum, D.B. Using citizen science to expand the global map of landslides: Introducing the Cooperative Open Online Landslide Repository (COOLR). *PLoS ONE* **2019**, *14*, e0218657. [[CrossRef](#)] [[PubMed](#)]
33. Kirschbaum, D.; Stanley, T.; Zhou, Y. Spatial and temporal analysis of a global landslide catalog. *Geomorphology* **2015**, *249*, 4–15. [[CrossRef](#)]
34. Kirschbaum, D.B.; Adler, R.; Hong, Y.; Hill, S.; Lerner-Lam, A. A global landslide catalog for hazard applications: Method, results, and limitations. *Nat. Hazards* **2010**, *52*, 561–575. [[CrossRef](#)]
35. Meena, S.R.; Puliero, S.; Bhuyan, K.; Floris, M.; Catani, F. Assessing the importance of conditioning factor selection in landslide susceptibility for the province of Belluno (region of Veneto, northeastern Italy). *Nat. Hazards Earth Syst. Sci.* **2022**, *22*, 1395–1417. [[CrossRef](#)]
36. Ado, M.; Amitab, K.; Maji, A.K.; Jasińska, E.; Gono, R.; Leonowicz, Z.; Jasiński, M. Landslide susceptibility mapping using machine learning: A literature survey. *Remote Sens.* **2022**, *14*, 3029. [[CrossRef](#)]
37. Pacheco Quevedo, R.; Velastegui-Montoya, A.; Montalván-Burbano, N.; Morante-Carballo, F.; Korup, O.; Daleles Rennó, C. Land use and land cover as a conditioning factor in landslide susceptibility: A literature review. *Landslides* **2023**, *20*, 967–982. [[CrossRef](#)]
38. Yang, H.; Adler, R.F. Predicting global landslide spatiotemporal distribution: Integrating landslide susceptibility zoning techniques and real-time satellite rainfall estimates. *Int. J. Sediment Res.* **2008**, *23*, 249–257.
39. Earth Resources Observation and Science (EROS) Center. *Courtesy of the US Geological Survey*; Earth Resources Observation and Science (EROS) Center: Reston, VA, USA, 2010.
40. Hartmann, J.; Moosdorf, N. The new global lithological map database GLiM: A representation of rock properties at the Earth surface. *Geochem. Geophys. Geosystems* **2012**, *13*, Q12004. [[CrossRef](#)]
41. Styron, R.; Pagani, M. The GEM global active faults database. *Earthq. Spectra* **2020**, *36*, 160–180. [[CrossRef](#)]
42. Beguería, S. Changes in land cover and shallow landslide activity: A case study in the Spanish Pyrenees. *Geomorphology* **2006**, *74*, 196–206. [[CrossRef](#)]
43. Niraj, K.; Singh, A.; Shukla, D.P. Effect of the normalized difference vegetation index (NDVI) on GIS-enabled bivariate and multivariate statistical models for landslide susceptibility mapping. *J. Indian Soc. Remote Sens.* **2023**, *51*, 1739–1756. [[CrossRef](#)]
44. Chen, L.; Guo, Z.; Yin, K.; Shrestha, D.P.; Jin, S. The influence of land use and land cover change on landslide susceptibility: A case study in Zhushan Town, Xuan'en County (Hubei, China). *Nat. Hazards Earth Syst. Sci.* **2019**, *19*, 2207–2228. [[CrossRef](#)]
45. Muñoz Sabater, J. *ERA5-Land Monthly Averaged Data from 1950 to Present*; Copernicus Climate Change Service (C3S) Climate Data Store (CDS): Bonn, Germany, 2019; Volume 10. [[CrossRef](#)]
46. Gorelick, N.; Hancher, M.; Dixon, M.; Ilyushchenko, S.; Thau, D.; Moore, R. Google Earth Engine: Planetary-scale geospatial analysis for everyone. *Remote Sens. Environ.* **2017**, *202*, 18–27. [[CrossRef](#)]
47. Wu, W.; Zhang, Q.; Singh, V.P.; Wang, G.; Zhao, J.; Shen, Z.; Sun, S. A data-driven model on Google earth engine for landslide susceptibility assessment in the Hengduan Mountains, the Qinghai–Tibetan plateau. *Remote Sens.* **2022**, *14*, 4662. [[CrossRef](#)]
48. Huang, F.; Xiong, H.; Jiang, S.-H.; Yao, C.; Fan, X.; Catani, F.; Chang, Z.; Zhou, X.; Huang, J.; Liu, K. Modelling landslide susceptibility prediction: A review and construction of semi-supervised imbalanced theory. *Earth-Sci. Rev.* **2024**, *250*, 104700. [[CrossRef](#)]
49. Pourghasemi, H.R.; Kornejady, A.; Kerle, N.; Shabani, F. Investigating the effects of different landslide positioning techniques, landslide partitioning approaches, and presence-absence balances on landslide susceptibility mapping. *CATENA* **2020**, *187*, 104364. [[CrossRef](#)]
50. Ngo, P.T.T.; Panahi, M.; Khosravi, K.; Ghorbanzadeh, O.; Kariminejad, N.; Cerda, A.; Lee, S. Evaluation of deep learning algorithms for national scale landslide susceptibility mapping of Iran. *Geosci. Front.* **2021**, *12*, 505–519.
51. Yao, J.; Qin, S.; Qiao, S.; Che, W.; Chen, Y.; Su, G.; Miao, Q. Assessment of landslide susceptibility combining deep learning with semi-supervised learning in Jiaohe County, Jilin Province, China. *Appl. Sci.* **2020**, *10*, 5640. [[CrossRef](#)]
52. Tien Bui, D.; Tuan, T.A.; Klempe, H.; Pradhan, B.; Revhaug, I. Spatial prediction models for shallow landslide hazards: A comparative assessment of the efficacy of support vector machines, artificial neural networks, kernel logistic regression, and logistic model tree. *Landslides* **2016**, *13*, 361–378. [[CrossRef](#)]

53. Zhang, Y.; Yan, Q. Landslide susceptibility prediction based on high-trust non-landslide point selection. *ISPRS Int. J. Geo-Inf.* **2022**, *11*, 398. [[CrossRef](#)]
54. Zhou, C.; Yin, K.; Cao, Y.; Ahmed, B.; Li, Y.; Catani, F.; Pourghasemi, H.R. Landslide susceptibility modeling applying machine learning methods: A case study from Longju in the Three Gorges Reservoir area, China. *Comput. Geosci.* **2018**, *112*, 23–37. [[CrossRef](#)]
55. Luo, X.; Lin, F.; Zhu, S.; Yu, M.; Zhang, Z.; Meng, L.; Peng, J. Mine landslide susceptibility assessment using IVM, ANN and SVM models considering the contribution of affecting factors. *PLoS ONE* **2019**, *14*, e0215134. [[CrossRef](#)] [[PubMed](#)]
56. Huang, W.; Ding, M.; Li, Z.; Zhuang, J.; Yang, J.; Li, X.; Meng, L.e.; Zhang, H.; Dong, Y. An efficient user-friendly integration tool for landslide susceptibility mapping based on support vector machines: SVM-LSM toolbox. *Remote Sens.* **2022**, *14*, 3408. [[CrossRef](#)]
57. Yang, J.; Ding, M.T.; Huang, W.B.; Li, Z.H.; Zhang, Z.Y.; Wu, J.; Peng, J.B. A generalized deep learning-based method for rapid co-seismic landslide mapping. *IEEE J. Sel. Top. Appl. Earth Obs. Remote Sens.* **2024**, *17*, 16970–16983. [[CrossRef](#)]
58. Shapley, L.S. A value for n-person games. In *Contributions to the Theory of Games II*; Princeton University Press: Princeton, NJ, USA, 1953; Volume 2.
59. Lundberg, S.M.; Lee, S.I. A unified approach to interpreting model predictions. *Adv. Neural Inf. Process. Syst.* **2017**, *30*, 4765–4774.
60. Pradhan, B.; Dikshit, A.; Lee, S.; Kim, H. An explainable AI (XAI) model for landslide susceptibility modeling. *Appl. Soft Comput.* **2023**, *142*, 110324. [[CrossRef](#)]
61. Molnar, C. *Interpretable Machine Learning*; Lulu.com: Raleigh, NC, USA, 2020.
62. Zhang, H.; Loaiciga, H.A.; Sauter, T. A novel fusion-based methodology for drought forecasting. *Remote Sens.* **2024**, *16*, 828. [[CrossRef](#)]
63. Mann, H.B. Nonparametric tests against trend. *Econom. J. Econom. Soc.* **1945**, *13*, 245–259. [[CrossRef](#)]
64. Kendall, M.G. *Rank Correlation Methods*; Charles Griffin and Co., Ltd.: London, UK, 1948.
65. Lin, Q.; Wang, Y. Spatial and temporal analysis of a fatal landslide inventory in China from 1950 to 2016. *Landslides* **2018**, *15*, 2357–2372. [[CrossRef](#)]
66. Zheng, H.; Ding, M. Spatiotemporal changes of landslide susceptibility in response to rainfall and its future prediction—A case study of Sichuan Province, China. *Ecol. Inform.* **2024**, *84*, 102862. [[CrossRef](#)]

Disclaimer/Publisher’s Note: The statements, opinions and data contained in all publications are solely those of the individual author(s) and contributor(s) and not of MDPI and/or the editor(s). MDPI and/or the editor(s) disclaim responsibility for any injury to people or property resulting from any ideas, methods, instructions or products referred to in the content.